Article

TRANSPARENT PROCESS OPEN ACCESS

THE EMBO JOURNAL

RBM14 prevents assembly of centriolar protein complexes and maintains mitotic spindle integrity

Gen Shiratsuchi[1], Katsuyoshi Takaoka[2], Tomoko Ashikawa[1], Hiroshi Hamada[2] & Daiju Kitagawa[1,*]

Abstract

Formation of a new centriole adjacent to a pre-existing centriole occurs only once per cell cycle. Despite being crucial for genome integrity, the mechanisms controlling centriole biogenesis remain elusive. Here, we identify RBM14 as a novel suppressor of assembly of centriolar protein complexes. Depletion of RBM14 in human cells induces ectopic formation of centriolar protein complexes through function of the STIL/CPAP complex. Intriguingly, the formation of such structures seems not to require the cartwheel structure that normally acts as a scaffold for centriole formation, whereas they can retain pericentriolar material and microtubule nucleation activity. Moreover, we find that, upon RBM14 depletion, a part of the ectopic centriolar protein complexes in turn assemble into structures more akin to centrioles, presumably by incorporating HsSAS-6, a cartwheel component, and cause multipolar spindle formation. We further demonstrate that such structures assemble in the cytoplasm even in the presence of pre-existing centrioles. This study sheds light on the possibility that ectopic formation of aberrant structures related to centrioles may contribute to genome instability and tumorigenesis.

Keywords cartwheel; centriole; centrosome; chromosome segregation; genome integrity

Subject Categories Cell Adhesion, Polarity & Cytoskeleton; Cell Cycle

DOI 10.15252/embj.201488979 | Received 15 May 2014 | Revised 11 September 2014 | Accepted 9 October 2014 | Published online 10 November 2014

The EMBO Journal (2015) 34: 97–114

Introduction

Centrosome duplication is tightly orchestrated with cell cycle progression to yield the correct number of centrosomes, which ensures robust formation of a mitotic bipolar spindle and faithful chromosome segregation (Nigg & Raff, 2009). The centrosome consists of a pair of centrioles surrounded by an electron-dense pericentriolar material (PCM). Formation of a new centriole adjacent to each pre-existing centriole is fundamental for centrosome duplication. Centriole formation starts with the assembly of a cartwheel structure onto which microtubules are then added (Brito *et al*, 2012; Gönczy, 2012). Besides this canonical pathway, the de novo formation of centrioles can be induced in the case of natural/physical loss of pre-existing centrioles (Marshall *et al*, 2001; Khodjakov *et al*, 2002; La Terra *et al*, 2005), in unfertilized Drosophila eggs overexpressing core centriole duplication factors (Peel *et al*, 2007; Rodrigues-Martins *et al*, 2007; Dzhindzhev *et al*, 2010; Stevens *et al*, 2010a), during early development in the mouse embryo (Courtois & Hiiragi, 2012) or in multicilia formation of terminally differentiated cells (Nigg & Raff, 2009). Although it is believed that the existence of pre-existing centrioles normally suppresses the *de novo* assembly in proliferating cells, exactly how this suppression is achieved remains unknown.

The SAS-6 family of proteins have been recently identified as crucial components of the cartwheel that is essential for centriole formation (Kilburn *et al*, 2007; Nakazawa *et al*, 2007; van Breugel *et al*, 2011; Kitagawa *et al*, 2011b). Moreover, human SAS-6 (HsSAS-6) overexpression induces formation of multiple procentrioles around a parental centriole, presumably through formation of multiple cartwheels (Strnad *et al*, 2007). Similar phenotypes have also been observed for overexpression of STIL (SCL/TAL1 interrupting locus) (Kitagawa *et al*, 2011a; Tang *et al*, 2011; Arquint *et al*, 2012; Vulprecht *et al*, 2012) and polo-like kinase 4 (Plk4) (Kleylein-Sohn *et al*, 2007), implying that there is a tight relationship between these critical components of the centriole assembly. In fact, in human cells, Plk4 acts upstream of HsSAS-6, regulating the presence of centriolar HsSAS-6 (Kleylein-Sohn *et al*, 2007; Strnad *et al*, 2007). In line with the fact that both HsSAS-6 and STIL localize to the proximal end of procentrioles (Kleylein-Sohn *et al*, 2007; Strnad *et al*, 2007; Tang *et al*, 2011; Arquint *et al*, 2012; Vulprecht *et al*, 2012), HsSAS-6 and STIL seem to be dependent on one another for their presence at procentrioles (Tang *et al*, 2011; Arquint *et al*, 2012; Vulprecht *et al*, 2012). HsSAS-6 and STIL are needed in turn for CPAP loading (Kohlmaier *et al*, 2009; Tang *et al*, 2009, 2011), which presumably promotes subsequent addition of centriolar microtubules and the elongation of procentrioles (Kohlmaier *et al*, 2009; Schmidt *et al*, 2009; Tang *et al*, 2009). Consistently, the induction of procentriole amplification by Plk4 overexpression is mediated by HsSAS-6 and STIL (Kleylein-Sohn *et al*, 2007; Tang *et al*, 2011; Arquint *et al*, 2012; Vulprecht *et al*, 2012). Given that the function of their relatives in centriole formation is evolutionarily conserved (Dammermann *et al*, 2004; Delattre *et al*, 2004; Leidel

1 Centrosome Biology Laboratory, Center for Frontier Research, National Institute of Genetics, Mishima, Shizuoka, Japan
2 Developmental Genetics Group, Graduate School of Frontier Biosciences, Osaka University, Suita, Osaka, Japan
*Corresponding author. Tel: +81 55 981 5828; E-mail: dkitagaw@nig.ac.jp

et al, 2005; Kilburn *et al*, 2007; Nakazawa *et al*, 2007; Rodrigues-Martins *et al*, 2007; Yabe *et al*, 2007; Culver *et al*, 2009; Stevens *et al*, 2010a) and that their relationship in other systems seems to be, at least in part, conserved (Delattre *et al*, 2006; Pelletier *et al*, 2006; Kitagawa *et al*, 2009; Stevens *et al*, 2010b), these three proteins are critical for the onset of centriole assembly. To conduct faithful centriole duplication, the function and expression levels of the critical components must be strictly regulated across the cell cycle.

In this study, we identify RNA-Binding Motif protein 14 (RBM14) as a STIL-interacting protein that interferes with a complex formation of STIL and CPAP. In addition, our data establish that RBM14 suppresses the formation of aberrant structures related to centrioles in the cytoplasm and thus preserves mitotic spindle integrity.

Results

Depletion of RBM14 induces ectopic formation of centriolar protein complexes

We set out to investigate the mechanisms limiting the number of newly formed centrioles. We reasoned that such regulators could physically interact with and directly control critical centriole proteins such as HsSAS-6 and STIL. Accordingly, we employed the mass spectrometry-based proteomic analysis to identify candidate proteins interacting with HsSAS-6 or STIL. Small-scale RNAi screening was subsequently conducted to address their function in centriole formation in human culture cells. This screening led to the identification of RNA-Binding Motif protein 14 (RBM14, also known as COAA, transcription co-activator, or PSP2, paraspeckle protein 2) (Iwasaki *et al*, 2001; Fox *et al*, 2002), a potential tumor suppressor conserved within vertebrates (Kang *et al*, 2008), as a STIL-interacting protein (Supplementary Table S1). We analyzed mitotic cells, which normally have four centrioles marked with centrin signals and assemble a bipolar spindle (Fig 1A). Intriguingly, we discovered that siRNA-mediated depletion of RBM14 resulted in a significant increase of centrin foci in human U2OS ($33 \pm 2\%$ compared with $7 \pm 2\%$ in control cells, $P < 0.01$, $n = 90$ in triplicate; Fig 1A and Supplementary Fig S1A), HeLa cells ($19 \pm 1\%$ compared with $1 \pm 1\%$ in control cells, $P < 0.01$, $n = 90$ in triplicate; Supplementary Fig S1B) and RPE1 cells ($17 \pm 4\%$ compared with $3 \pm 2\%$ in control cells, $P < 0.05$, $n = 90$ in triplicate; Supplementary Fig S1C). We also found a similar phenotype in interphase cells (Supplementary Fig S1D). The amplification of centrin foci was detectable within 24 h after siRNA transfection in U2OS cells without a significant cell cycle arrest or cytokinesis defect (Supplementary Fig S1E and F). It has been previously reported that RBM14 acts as a component of the nuclear paraspeckle and functions in RNA processing and transcription (Auboeuf *et al*, 2004). The nuclear paraspeckle is a small intranuclear structure that is known to contain RNA and several ribonucleoproteins. We therefore assessed the possibility that RBM14 depletion somehow affects centriole formation through transcriptional regulation. However, mis-localization of RBM14 from the paraspeckle caused by depletion of p54nrb/NONO, a protein essential for paraspeckle organization (Sasaki *et al*, 2009), did not induce amplification of centriole foci (Supplementary Fig S1H). In addition, expression levels of STIL and other centriole proteins were unaffected by RBM14 depletion (Supplementary Figs S1A, S4A, S5A, and S9B). Furthermore, incubation with 0.5 mM cycloheximide, a translation inhibitor, did not suppress excess formation of centrin foci by RBM14 depletion (Supplementary Fig S1G). Based on these observations, we conclude that the amplification of centrin foci by RBM14 depletion likely stems from reduction of unknown function of RBM14 rather than its known function as a component of the nuclear paraspeckle.

Next, to distinguish whether the amplification of centrin foci is because of multiple rounds of centriole duplication or concurrent formation of multiple procentrioles and/or procentriole-like premature structures, we monitored the number of C-Nap1 or Cep164-labeled parental centrioles (Fry *et al*, 1998; Graser *et al*, 2007) and Centrobin, a procentriole marker (Zou *et al*, 2005), foci in mitotic RBM14-depleted cells. We found that $31 \pm 4\%$ of the cells harbored an increased number of Centrobin foci ($P < 0.05$, $n = 90$ in triplicate; Fig 1B), whereas the number of parental centrioles was not statistically affected compared with control cells (Fig 1A and Supplementary Fig S1I). These results indicate that the ectopic centrin foci in RBM14-depleted cells likely represent amplification of procentrioles or procentriole-like premature structures, or both, rather than multiple rounds of centriole duplication.

We also noted that most of these structures contained other centriolar proteins such as CPAP (Hung *et al*, 2000) ($65 \pm 3\%$, $n = 150$ in triplicate; Supplementary Fig S1J) and CP110 (Chen *et al*, 2002) ($55 \pm 3\%$, $n = 150$ in triplicate; Supplementary Fig S1J) that constitute the middle-distal parts of centrioles. Consistently, we found significant increase in the number of CPAP and CP110 foci in the cells depleted of RBM14 ($23 \pm 2\%$ compared with 0% in control cells, $30 \pm 2\%$ compared with $6 \pm 2\%$ in control cells, respectively; for both cases, $P < 0.01$, $n = 90$ in triplicate; Fig 1C and Supplementary Fig S1K). Furthermore, we observed ectopic foci of acetylated tubulin in the cells depleted of RBM14 ($11 \pm 1\%$ compared with $1 \pm 1\%$ in control cells, $P < 0.01$, $n = 90$ in triplicate; Fig 1D) and also found that some of ectopic centrin-containing structures appeared to incorporate acetylated tubulin ($26 \pm 2\%$, $n = 150$ in triplicate; Supplementary Fig S1J), suggesting that they contain the centriolar microtubules. We next tested whether the ectopic centrin-containing structures are functional enough to assemble PCM. Upon depletion of endogenous RBM14, the ectopic centrin-containing structures efficiently accumulated PCM proteins such as γ-tubulin and Cep192 (Stearns *et al*, 1991; Zheng *et al*, 1991; Gomez-Ferreria *et al*, 2007; Zhu *et al*, 2008) ($39 \pm 2\%$ and $41 \pm 2\%$, respectively, $n = 150$ in triplicate; Supplementary Fig S1J). In line with this, we found significant increase in the number of ectopic PCM formation ($22 \pm 3\%$ compared with $4 \pm 1\%$ in control cells for γ-tubulin, $P < 0.01$, $n = 90$ in triplicate; $22 \pm 2\%$ compared with $3 \pm 2\%$ in control cells for Cep192, $P < 0.05$, $n = 90$ in triplicate; Fig 1E and Supplementary Fig S1L). Based on these observations, we refer to the ectopic structures containing centriolar proteins and induced in RBM14-depleted cells as "centriolar protein complexes" in this article.

Cytoplasmic RBM14 can inhibit centriole amplification in cells arrested in S phase

To confirm that the appearance of ectopic centriolar protein complexes specifically results from loss of RBM14 and also to

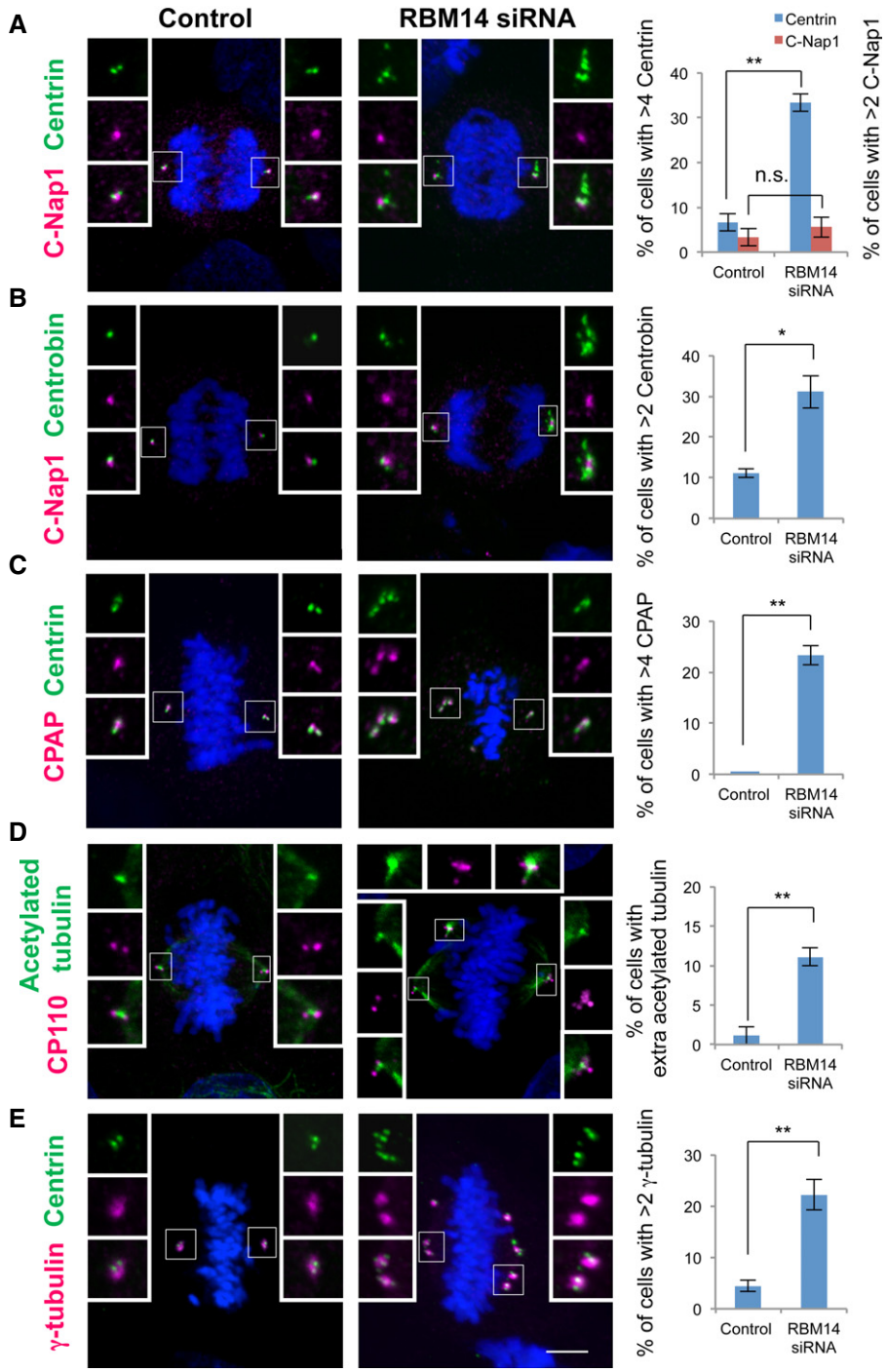

Figure 1. Depletion of RBM14 induces ectopic formation of centriolar protein complexes.

A–E Mitotic control U2OS cells or U2OS cells treated with RBM14 siRNA were stained with antibodies against centrin-2 (green) and C-Nap1 (magenta) (A), Centrobin (green) and C-Nap1 (magenta) (B), centrin-2 (green) and CPAP (magenta) (C), acetylated-tubulin (green) and CP110 (magenta) (D), and centrin-2 (green) and γ-tubulin (magenta) (E). DNA is shown in blue. Insets show approximately twofold magnified views of fluorescent foci around the centrosome. Scale bar, 5 μm. Histograms on the right represent frequency of mitotic cells with excess foci of the indicated proteins at spindle poles in each condition. Values are mean percentages ± standard error of mean (SEM) from three independent experiments (n = 30 for each condition). *$P < 0.05$, **$P < 0.01$, n.s., not significant (one-tailed t-test). Note that we counted the number of C-Nap1 foci after anaphase in mitosis when C-Nap1 signals recover from the reduction in prometaphase.

identify the region of RBM14 required for its function, we tested whether full-length (FL) and/or fragments of RBM14 can rescue the phenotype provoked by treatment with siRNA against the 3′ UTR targeting solely endogenous RBM14. We found that expression of the C-terminal half of RBM14 (RBM14[C]) lacking the RNA-recognition motif (RRM) as well as RBM14 FL markedly suppressed the amplification

of centriolar protein complexes in the cells depleted of endogenous RBM14 (Fig 2A and B, and Supplementary Fig S2A).

Next, to further investigate the function of RBM14 in normal centriole formation or centriole re-duplication in cells arrested in S phase, we ectopically expressed RBM14 FL and RBM14[C] in U2OS cells. Although overexpression of RBM14 had only a minor effect on normal centriole duplication and PCM assembly (Supplementary Fig S2B and C) or formation of multiple procentrioles induced by overexpression of Plk4, STIL or HsSAS-6 (Supplementary Fig S2D), we found that it significantly inhibited centriole amplification in cells treated with hydroxyurea (HU) to prolong S phase, judged by the frequency of cells with more than 4 centrin foci (26 ± 3% in cells expressing RBM14 FL, 27 ± 2% in cells expressing RBM14[C] compared with 53 ± 4% in control cells, $P < 0.05$, $n = 90$ in triplicate; Fig 2C). We noted in addition that ectopically expressed RBM14 FL proteins mainly existed in the nucleus, but also localized in the cytoplasm as is the case for the endogenous proteins (Fig 2C and Supplementary Fig S2A, E and F). By contrast, we found that RBM14[C] could occasionally localize in the vicinity of centrioles during interphase (14.4 ± 2.9% compared with 2.2 ± 1.1% of RBM14 FL and 1.1 ± 1.1% of endogenous RBM14, $n = 90$; Fig 2C and Supplementary Fig S2E), implying that this region may bind to a centriolar protein. These observations prompted us to investigate where RBM14 could act on centriole biogenesis. To address this, we manipulated the localization of RBM14 by fusing NES (nuclear export signal) or PACT domain, a centrosomal targeting motif, to

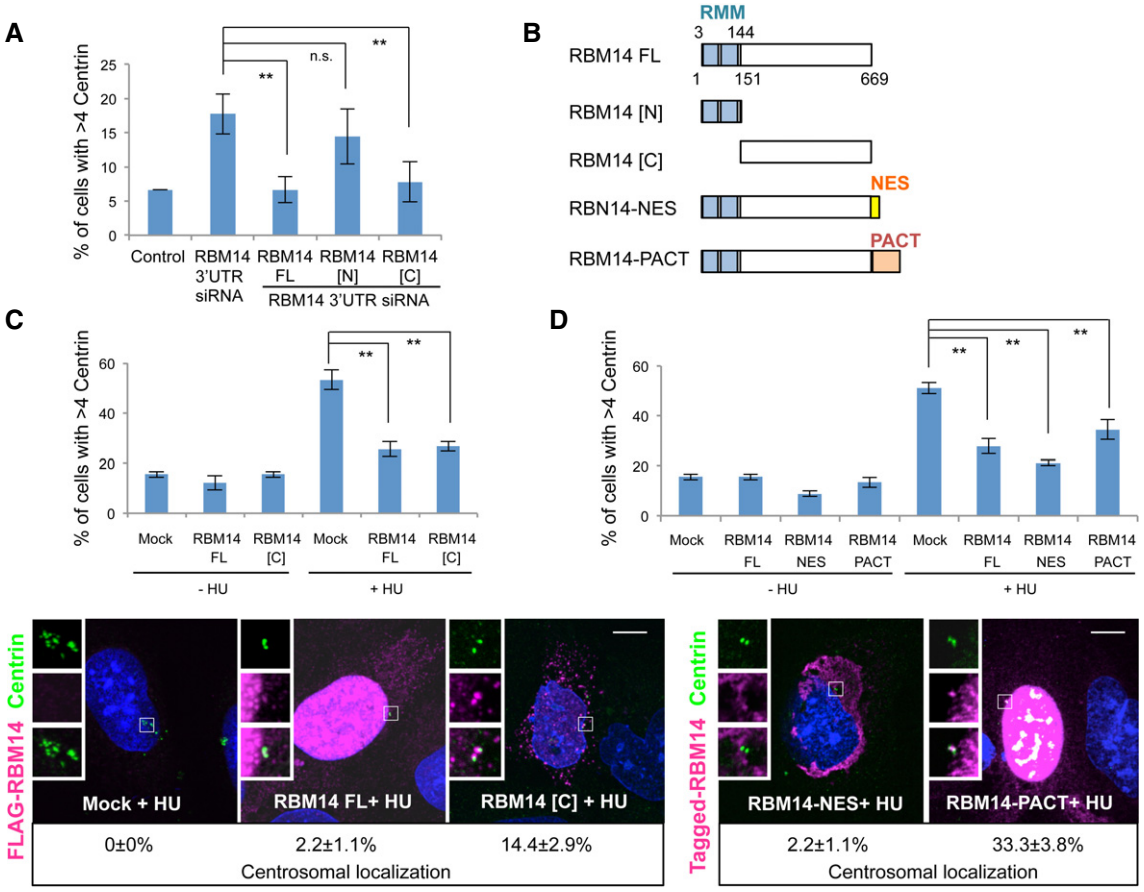

Figure 2. RBM14 can suppress centriole amplification in cells arrested in S phase.

A U2OS cells or U2OS cells expressing FLAG–RBM14 full length (FL, aa1–669), N-terminal fragment (RBM14[N], aa1–150) or C-terminal fragment (RBM14[C], aa151–669) and treated with control siRNA or siRNA against 3′ UTR targeting endogenous RBM14 were stained with antibodies against FLAG as well as centrin-2. Histograms represent frequency of mitotic cells with excess centrin foci at spindle poles in each condition. Values are mean percentages ± SEM from three independent samples ($n = 30$ for each condition). $^{**}P < 0.01$, n.s., not significant (one-tailed *t*-test).

B Schematic of full-length, truncated mutants and NES-fused and PACT-fused RBM14 proteins used in this figure.

C, D Cytoplasmic RBM14 could suppress centriole amplification in HU-treated cells. (C) U2OS cells or U2OS cells expressing FLAG-RBM14 FL or [C] and treated with or without HU were stained with antibodies against centrin-2 (green) and FLAG (magenta). (D) U2OS cells or U2OS cells expressing FLAG-RBM14 FL, FLAG-RBM14-NES or GFP-RBM14-PACT and treated with or without HU were stained with antibodies against FLAG (magenta, left) or GFP (magenta, right) as well as centrin-2 (green). Insets show approximately twofold magnified views of fluorescent foci around the centrosome. Scale bar, 10 μm. Histograms represent frequency of cells in interphase with excess centrin foci in each condition. The percentages of U2OS cells with centrosomal localization of the RBM14 full-length protein or mutants are shown below the immunofluorescence images. We counted only cells that had adequate intensity of FLAG or GFP signals and did not find any significant difference in the total expression levels of the exogenous RBM14 proteins. Values are mean percentages ± SEM from three independent experiments ($n = 30$ for each condition). $^{**}P < 0.01$ (one-tailed *t*-test). Please note that cytoplasmic expression levels of GFP-RBM14-PACT are less than those of FLAG-RBM14 FL (~0.5-fold) or FLAG-RBM14-NES (~0.7-fold).

the C-terminal end of RBM14 (Fig 2B). Intriguingly, we found that when overexpressing RBM14-NES which localized to the cytoplasm, but seemingly not to centrioles (only 2.2 ± 1.1% of RBM14-NES in the vicinity of centrioles during interphase, $n = 90$; Fig 2D), HU-induced centriole amplification was efficiently suppressed as is the case for overexpression of the native full-length protein (21 ± 1% in cells expressing RBM14-NES compared with 28 ± 3% in cells expressing RBM14, $P < 0.05$, $n = 90$ in triplicate; Fig 2D). On the other hand, overexpression of RBM14-PACT localizing to centrioles (33.3 ± 3.8%, $n = 90$; Fig 2D) and in the cytoplasm also suppressed the centriole amplification, but not more effectively (34 ± 4%, $n = 90$ in triplicate; Fig 2D), suggesting that the centriolar loading of RBM14 itself seems not to be essential for its ability to suppress centriole amplification. Furthermore, we established that expression of RBM14-NES suppressed the phenotype provoked by depletion of endogenous RBM14 (Supplementary Fig S2G). Overall, these data lead us to propose that cytoplasmic localization of RBM14 is crucial for its function to suppress amplification of centrioles or ectopic centriolar protein complexes.

RBM14 interacts with STIL and prevents a complex formation of STIL and CPAP

We next confirmed by co-immunoprecipitation experiments with the endogenous proteins that RBM14 is a *bona fide* STIL-binding protein *in vivo* (Fig 3A and Supplementary Fig S3A). On the other hand, we could not detect interaction between endogenous STIL and CPAP proteins in these experiments. Moreover, yeast two-hybrid, GST pull-down and co-immunoprecipitation assays using full-length and fragments of STIL and RBM14 established that the N-terminal region of STIL (STIL[N]) directly bound to the C-terminal region of RBM14, which is crucial for the ability of RBM14 to suppress the formation of ectopic centriolar protein complexes (Fig 3B and C, and Supplementary Fig S3B–D). Furthermore, using GST pull-down assays with several deletion mutants of RBM14[C], we determined that the TRBP (thyroid hormone receptor-binding protein)/Ncoa6-interacting domain (307–584 aa) (Iwasaki *et al*, 2001) is responsible for STIL–RBM14 binding (Fig 3C and Supplementary Fig S3E and F). This domain is composed of a serine/alanine/glycine/tyrosine-rich region and thought to be a protein–protein binding domain of RBM14. Consistently, functional analysis revealed that expression of the RBM14 mutant proteins that lack the TRBP-interacting domain did not efficiently rescue the phenotype provoked by depletion of endogenous RBM14 (Supplementary Fig S3G), suggesting that direct binding of RBM14 to STIL through the TRBP-interacting domain is required for the function of RBM14 suppressing ectopic formation of centriolar protein complexes. These data prompted us to examine whether this interaction influences the expression levels or centriolar localization of STIL, or both. However, both immunofluorescence and Western blot analyses in RBM14-depleted U2OS cells showed that fluctuating expression at centrioles and total expression levels of STIL across the cell cycle (Tang *et al*, 2011; Arquint *et al*, 2012; Vulprecht *et al*, 2012) seemed comparable to the control (Fig 3D and Supplementary Fig S4A). There was also no alteration in the localization of STIL at the proximal end of procentrioles (Tang *et al*, 2011; Arquint *et al*, 2012; Vulprecht *et al*, 2012) (G. Shiratsuchi, D. Kitagawa, unpublished observation). However, we noted that relatively small ectopic centrin foci, but not seemingly mature centrin foci, tended to contain STIL signals during mitosis (9 ± 3% for RBM14-depleted cells, 1 ± 1% for control cells, $P < 0.05$, $n = 90$ in triplicate; Fig 3D), implying that STIL could localize to premature centriolar protein complexes only transiently. Based on these data, we postulated that the binding of RBM14 to STIL might affect the function of STIL in centriole formation. Given that STIL[N] contained the region responsible for CPAP-binding (231–781 aa) (Tang *et al*, 2011), we assumed that RBM14 may disrupt the interaction between STIL and CPAP. To address this, we conducted *in vitro* pull-down assay to test whether RBM14[C] and the STIL-binding region of CPAP, CPAP [SBD], compete with each other for binding to STIL[N]. We found this to be the case, supporting the model in which RBM14 prevents the formation of STIL/CPAP complex (Fig 3E). Furthermore, we found that addition of RBM14 FL or RBM14[C], but not RBM14[N], efficiently dampened the complex formation of STIL and GFP-CPAP in U2OS cells (Fig 3F). These findings are in line with the fact that the C-terminal region of RBM14 is responsible for STIL binding (Fig 3B and C, and Supplementary Fig S3). Importantly, we revealed, using siRNA-based double knockdown experiments, that the formation of ectopic centrin foci by RBM14 depletion depends on CPAP and STIL (Fig 3G). Moreover, to further confirm the biological relevance of the complex formation of STIL and CPAP in this process, we tested whether expression of STIL mutants, STIL[N] and STIL[CBD], that contain CPAP-binding domain (CBD), but lack the conserved STAN motif, could act in a dominant-negative manner to inhibit the formation of the ectopic centriolar protein complexes in RBM14-depleted cells. Accordingly, we found that this was indeed the case (Supplementary Fig S4B). Overall, these findings lead us to propose that the interaction of RBM14 with STIL suppresses the inherent ability of the STIL/CPAP complex for the ectopic formation of centriolar protein complexes.

The ectopic formation of centriolar protein complexes occurs in the cytoplasm in a HsSAS-6-independent manner

Next, to test the dependency of a cartwheel structure on the formation of ectopic centriolar protein complexes, we conducted RNAi-mediated reduction of HsSAS-6 in the RBM14-depleted cells. Strikingly, this analysis revealed that the formation of ectopic centrin foci was mostly independent of the existence of HsSAS-6 (Fig 4A and Supplementary Fig S5A and B). Similarly, depletion of Plk4 did not affect the amplification of centriolar protein complexes (Supplementary Fig S5C). These results suggest that the amplification of centriolar protein complexes induced by RBM14 depletion occurs independently of HsSAS-6 and possibly of a cartwheel structure. We also observed that assembly of PCM components was not critical for this process (Supplementary Fig S5D) even though we somehow detected the interaction of RBM14[C] with γ-tubulin (Supplementary Fig S5E).

To investigate when and how the ectopic structures are formed, we employed long-term fluorescence time-lapse recording with HeLa cells stably expressing GFP-centrin (Piel *et al*, 2000) and depleted of RBM14. Intriguingly, we found that the ectopic GFP-centrin foci were formed in the cytoplasm (Fig 4B and Supplementary Movie S1). Our automated particle analysis demonstrated that the number of centrin foci whose signal intensity rose above the threshold was gradually increased and reached saturation (4.8 ± 0.7 in RBM14-depleted cells compared with 1.6 ± 0.4 in

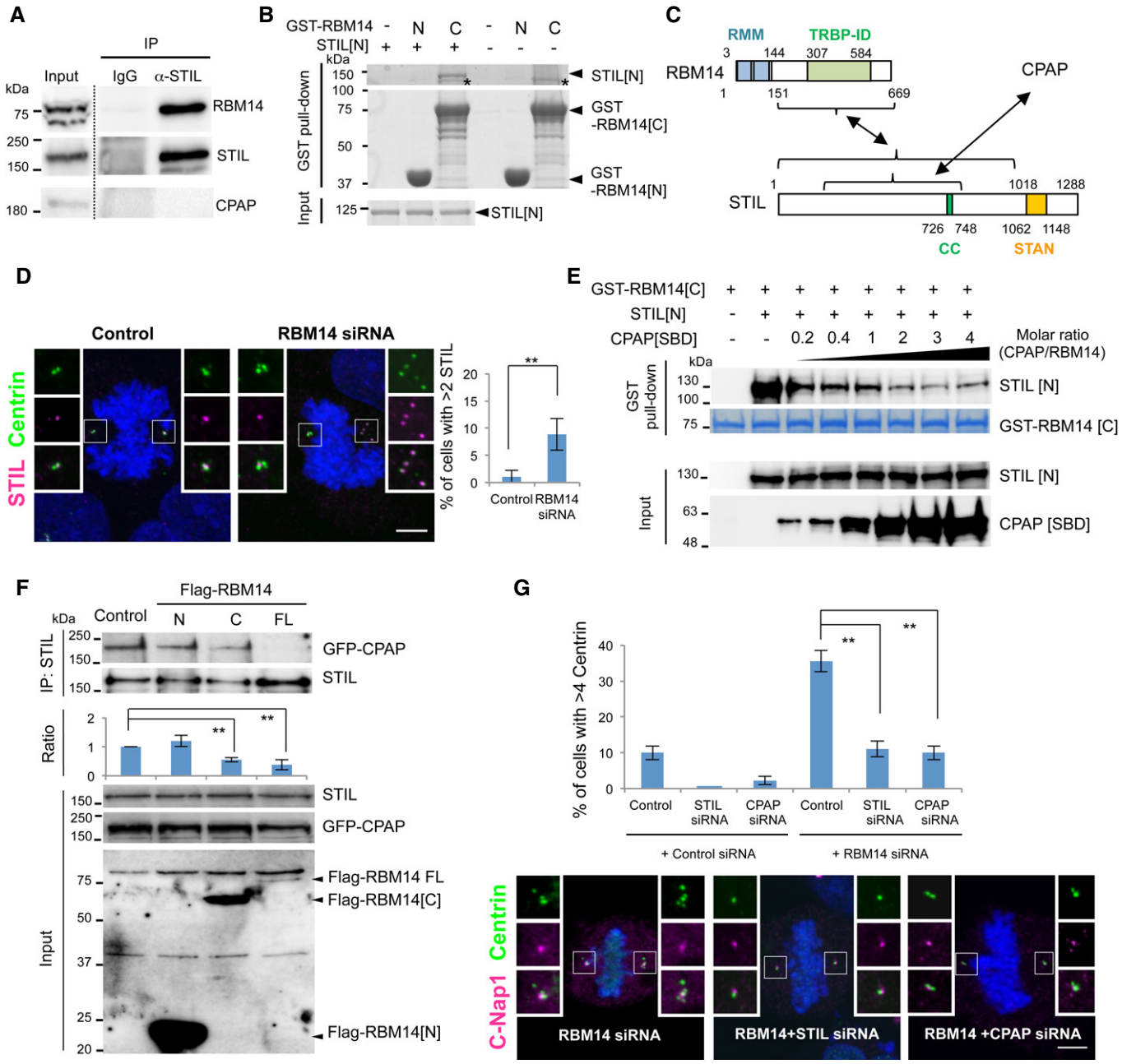

Figure 3.

control cells, respectively, $n = 5$; Fig 4B) within approximately 3 h from the appearance of the foci. Importantly, further detailed observation of the behavior of individual foci revealed that some small centrin foci in the cytoplasm fused with each other and grew to a size comparable to the centrin foci of pre-existing centrioles (Supplementary Movies S2 and S3). On the other hand, the signal intensities and pattern of centrin foci at pre-existing centrioles were not altered, suggesting that formation of ectopic centrin foci was not because of fragmentation of pre-existing centrioles. We also noted that such ectopic formation of centrin foci was unlikely dependent on microtubules (Supplementary Fig S5F). Moreover, such assembly of ectopic centrin foci seemed to occur approximately from late G1 to S phase (Fig 4C and Supplementary Movie S4). Indeed, cell cycle arrest experiments and PCNA staining in RBM14-depleted U2OS cells confirmed that ectopic formation of centriolar protein complexes occurred during S phase (Fig 4D and Supplementary Fig S5G and H). Lovastatin-induced G1 phase arrest significantly inhibited amplification of centriolar protein complexes, whereas HU-induced S phase arrest did not suppress the phenotype.

These data prompted us to analyze the morphological features of the ectopic centriolar protein complexes in RBM14-depleted cells at the ultrastructural level using transmission electron microscopy (TEM). Repeated TEM analysis revealed that most of the structures corresponded to amorphous electron-dense materials (white squares in Fig 4E and Supplementary Fig S5I). The average diameter of these structures (130 ± 11 nm, $n = 16$) is shorter than pre-existing

Figure 3. RBM14 interacts with STIL and prevents a complex formation of STIL and CPAP.

A HeLa cells immunoprecipitated with control IgG or STIL antibodies. Soluble cytosolic fractions (input) and immunoprecipitates (IPs) were analyzed by Western blotting using RBM14, STIL or CPAP antibodies.

B GST pull-down assay testing interactions between purified STIL[N] (~5 μg, aa1–1018) and GST-RBM14 [N] or [C]. The asterisks indicate non-specific bands.

C Schematic of our analyses of Y2H, GST pull-down and co-immunoprecipitation of the interaction between RBM14 and STIL (see also Supplementary Fig S3). Brackets indicate the fragments tested in this study, and the interaction detected is shown with arrows. A previous study reported that the C-terminus of CPAP interacts with the fragment of STIL aa231–781, as indicated (Tang *et al*, 2011).

D Mitotic U2OS cells treated with control or RBM14 siRNA were stained with antibodies against centrin-2 (green) and STIL (magenta). Insets show approximately twofold magnified views of fluorescent foci around the centrosome. Scale bar, 5 μm. Histograms represent frequency of mitotic cells with excess STIL foci co-localized with centrin foci. Values are mean percentages ± SEM from three independent samples (n = 30 for each condition). $^{**}P < 0.01$ (one-tailed t-test).

E *In vitro* competitive binding assay. GST pull-down experiment was performed as in (B), with purified STIL[N] and GST-RBM14[C] in the presence of the indicated amount of purified His-CPAP[SBD], His-tagged STIL-Binding Domain of CPAP. The fraction of STIL[N] bound to GST-RBM14[C] in such conditions was monitored by Western blotting using STIL antibodies which recognize the N-terminal region of STIL. Input materials were analyzed by Western blotting using the STIL or CPAP antibodies. The precipitated GST-RBM14[C] was analyzed by SDS–PAGE, stained with SimplyBlue™ Safe (Invitrogen).

F Interaction between STIL and GFP-CPAP in the presence of FLAG-RBM14 FL or fragments. U2OS cells expressing GFP-CPAP were transfected with empty vector as a control, FLAG-RBM14[N], FLAG-RBM14[C] or FLAG-RBM14 FL constructs, immunoprecipitated with STIL antibodies, and the resulting IPs were analyzed by Western blotting using STIL, CPAP or FLAG antibodies. Quantification of relative protein amounts of co-immunoprecipitated GFP-CPAP in each STIL-IP fraction, normalized with the amount of STIL precipitated, is shown below the panels. Means ± SEM were calculated from three independent experiments. $^{**}P < 0.01$ (one-tailed t-test). Note that we did not find any significant effect of exogenous expression of RBM14 full-length protein or deletion mutants on the expression levels of GFP-CPAP or endogenous STIL proteins in this experiment.

G U2OS cells treated with the indicated siRNAs were stained with antibodies against centrin-2 (green) and C-Nap1 (magenta). Histograms represent frequency of mitotic cells with excess centrin foci at spindle poles in each condition. Values are mean percentages ± SEM from three independent experiments (n = 30 for each condition). $^{**}P < 0.01$ (one-tailed t-test). Representative mitotic cells treated with siRNAs against RBM14 alone, RBM14 + STIL or RBM14 + CPAP are shown below. Insets show approximately twofold magnified views of fluorescent foci around the centrosome. Scale bar, 5 μm.

centrioles (225 ± 8 nm, n = 10). Some amorphous structures contained microtubule structures, although they were not cylindrically arranged (Fig 4E). CLEM (Correlative Light Electron Microscopy) analysis further confirmed that the amorphous structures contained CPAP that is a critical component of ectopic centriolar protein complexes in RBM14-depleted cells (Fig 4F and G). In addition, although it has been shown that the centriolar satellites can be morphologically detected as small electron-dense granules that surround centrosomes, the ectopic centriolar protein complexes in RBM14-depleted cells did not co-localize with foci of PCM-1, a major centriolar satellite protein (Balczon *et al*, 1994) (Supplementary Fig S5J). Overall, these results show that, upon RBM14 depletion, the amorphous centriolar protein complexes formed in the cytoplasm during S phase in a HsSAS-6-independent manner.

Ectopic centriolar protein complexes can be the sites of microtubule nucleation

Since the ectopic centriolar protein complexes induced by RBM14 depletion could recruit PCM components (Fig 1E), we next tested whether they are potent to nucleate microtubules. Given that formation of the centriolar protein complexes frequently resulted in pseudo-bipolar spindle formation in which an abnormal number of centriolar protein foci clustered into spindle poles, we sought to establish an experimental setup in which it is possible to decluster the centriolar protein complexes and pre-existing centrioles and evaluate their ability to nucleate microtubules in mitosis. To this end, we carried out a microtubule regrowth assay using mitotic U2OS cells (Fig 5A). As expected, in control mitotic cells, we detected efficient microtubule regrowth and subsequent spindle formation within 30 min after cold treatment (Fig 5B). Importantly, we found that, upon RBM14 depletion, the ectopic centriolar protein complexes with PCM cloud formed extra spindle poles, which often induced formation of multipolar spindles at 30 min after cold treatment (Fig 5C–E). 46 ± 5% of the centriolar protein complexes appeared to harbor microtubule nucleation activity in mitosis (n = 150 in triplicate). However, we observed that extra small spindle poles in RBM14-depleted cells tended to be clustered into a pseudo-bipolar spindle assay at 60 min after cold treatment (Fig 5C). Taken together, these results indicate that the ectopic centriolar protein complexes induced by RBM14 depletion are at least in part potent to nucleate microtubules.

Ectopic centriolar protein complexes can assemble into structures more akin to procentrioles

We next sought to analyze the molecular components of the ectopic centriolar protein complexes that can organize a mitotic spindle. In line with the observation in the microtubule regrowth assays (Fig 5), we first confirmed that there was an increase in the frequency of multipolar spindle formation in RBM14-depleted cells (~9% for RBM14-depleted HeLa cells and ~2% for the control cells, respectively, $n \geq 44$; 7 ± 2% for RBM14-depleted U2OS cells compared with 0% for the control cells, $P < 0.05$, n = 90 in triplicate; Supplementary Fig S6A and B). Furthermore, we found that most of the cells depleted of RBM14 and with multipolar spindles harbored extra HsSAS-6 foci and acetylated-tubulin foci (Fig 6A and Supplementary Fig S6C). Consistently, we noted that only a small but statistically significant portion of the RBM14-depleted cells exhibited excess foci of HsSAS-6 overlapping with the ectopic centrin foci (8 ± 1% compared with 2 ± 1% in control cells, $P < 0.05$, n = 90 in triplicate; Fig 6B and Supplementary Fig S6D). These ectopic centriolar protein complexes containing HsSAS-6 appeared to co-localize with Cep135/Bld10p and Cep152/Asterless (80 ± 2% and 78 ± 1%, respectively, n = 90 in triplicate; Supplementary Fig S6E) both of which are presumably implicated in the early stage of procentriole formation (Kleylein-Sohn *et al*, 2007) (Blachon *et al*, 2008). Moreover, we found that HsSAS-6 depletion substantially offsets the increase in the frequency of the cells with multipolar spindle formation in RBM14-depleted cells (Fig 6C). In contrast, most pseudo-bipolar spindles in which an abnormal number of centrin foci clustered into two spindle poles did not

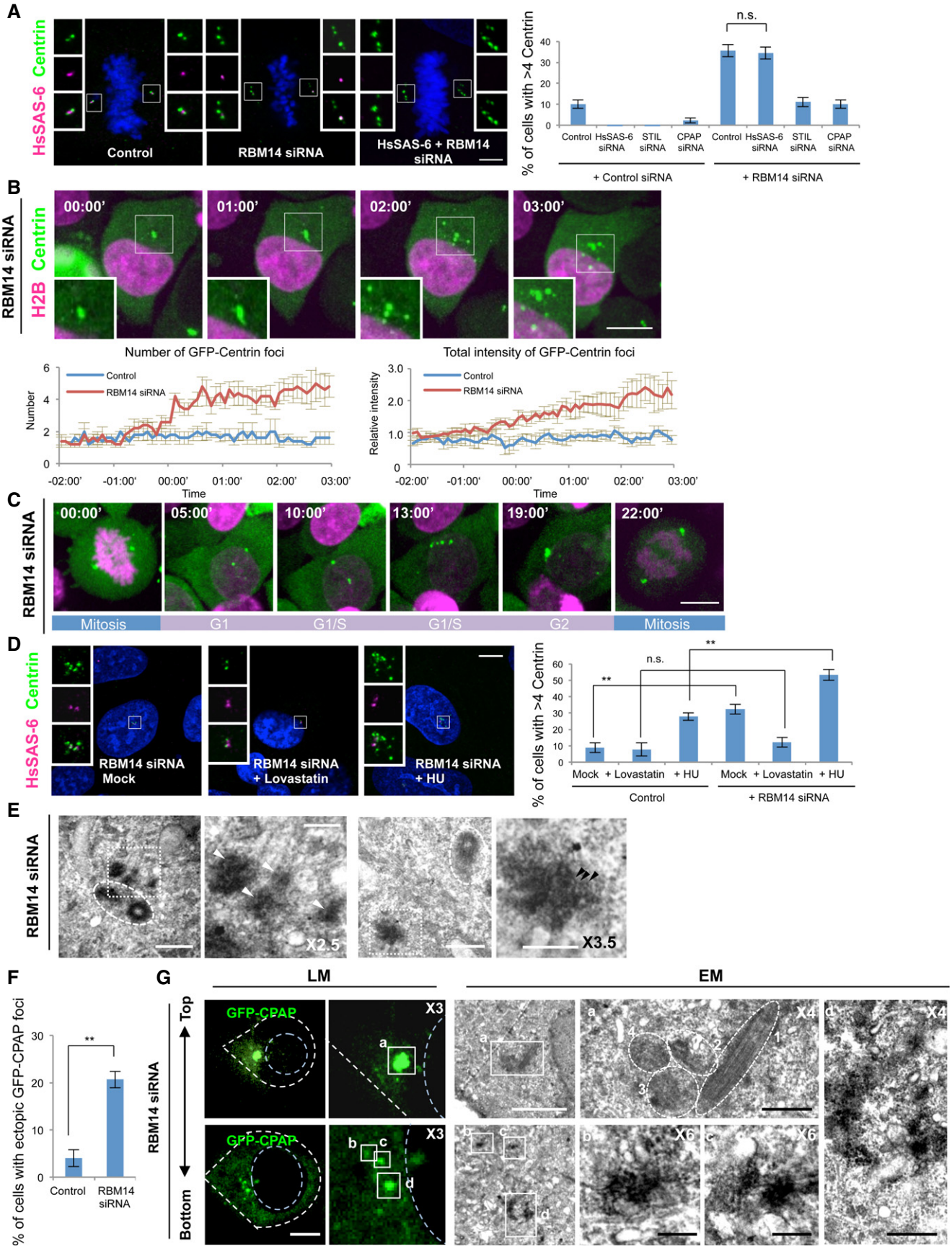

Figure 4.

Figure 4. HsSAS-6-independent formation of centriolar protein complexes occurs in the cytoplasm in RBM14-depleted cells.

A U2OS cells treated with control siRNA, RBM14 siRNA alone or RBM14 + HsSAS-6 siRNAs were stained with antibodies against centrin-2 (green) and HsSAS-6 (magenta). DNA is shown in blue. Insets show approximately twofold magnified views of fluorescent foci around the centrosome. Scale bar, 5 μm. Histograms represent frequency of mitotic cells with excess centrin foci in the indicated conditions. Values are mean percentages ± SEM from three independent experiments (n = 30 for each condition). n.s., not significant (one-tailed t-test).

B Live imaging of cycling RBM14-depleted HeLa cells expressing GFP-centrin1 (green) and RFP-H2B (magenta). Insets show approximately 1.5-fold magnified images of fluorescent foci. Time is denoted in hh:min, and scale bar is 10 μm. Time zero corresponds to the onset of excess centrin foci formation. Quantification of the number and total signal intensity of centrin foci in HeLa cells treated with control or RBM14 siRNA over time. Means ± SEM are shown (n = 5).

C Ectopic formation of centriolar intermediates likely occurs from late G1 to S phase. Time-lapse recording across the cell cycle of HeLa cells expressing GFP-centrin (green) and RFP-H2B (magenta) and treated with RBM14 siRNA. Time is denoted in hh:min, and scale bar is 10 μm. Time zero corresponds to the metaphase onset.

D Ectopic formation of centriolar protein complexes occurs during S phase arrest induced by HU treatment but not G1 phase arrest induced by lovastatin treatment. Insets show threefold magnified images of fluorescent foci. Scale bar, 5 μm. Histograms represent frequency of mitotic cells with excess centrin foci in the indicated conditions. Values are mean percentages ± SEM from three independent experiments (n = 30 for each condition). $^{**}P < 0.01$, n.s., not significant (one-tailed t-test).

E Amorphous electron-dense structures containing microtubules are formed in RBM14-depleted cells (see also Supplementary Fig S5I). Electron micrographs from U2OS cells depleted of RBM14. Squares indicate the ectopic electron-dense structures, whereas circles indicate the pre-existing centrioles. Scale bar, 500 nm and 200 nm (magnified views). Average diameter of pre-existing centrioles and the amorphous electron-dense structures are 225 ± 8 nm (n = 10) and 130 + 11 nm (n = 16), respectively. Insets show magnified views of the squares. Note that microtubules (black arrowheads) are observed within the electron-dense structures (white arrowheads).

F Histograms represent frequency of the cells with ectopic foci of GFP-CPAP in the indicated conditions. U2OS cells expressing GFP-CPAP were fixed and stained 24 h after RNAi treatment and induction of GFP-CPAP. Values are mean percentages ± SEM from three independent experiments (n = 30 for each condition). $^{**}P < 0.01$ (one-tailed t-test).

G U2OS cells expressing GFP-CPAP (green) and treated with RBM14 siRNA were analyzed using CLEM. Separate z-plane images of the cell with GFP-CPAP foci and the threefold magnified images are aligned from bottom to top along z-axis (left LM panels). White broken lines represent cell shapes, and blue broken lines represent nuclear shapes. Corresponding regions of EM images are shown on the right. White squares (a–d) represent the region around GFP-CPAP foci. Note that other than pre-existing centrioles (a, 1–4), ectopic small CPAP foci are recognizable as amorphous electron-dense structures (b–d). One of pre-existing centrioles (1) is elongated because of exogenous GFP-CPAP expression. Scale bar, 10 μm (LM), 2 μm (EM, low magnified image), 500 nm [magnified images of (a) and (d)), 200 nm (magnified images of (b) and (c)].

contain extra HsSAS-6 or acetylated-tubulin foci (n = 44; Fig 6A and Supplementary Fig S6C). Together, these results suggest that the ectopic centriolar protein complexes that have incorporated HsSAS-6 become more potent for spindle assembly.

Next, we further investigated the molecular components of HsSAS-6-containing centriolar protein complexes by conducting triple-labeling immunofluorescence analysis with HeLa cells expressing GFP-centrin. Intriguingly, this experiment revealed that HsSAS-6-containing centriolar protein complexes presented almost appropriate placement of HsSAS-6, centrin and CP110 that mark the centriole proximal and distal ends (Kleylein-Sohn *et al*, 2007; Strnad *et al*, 2007) (Fig 6D). However, we found that the distance between the HsSAS-6 signal at the proximal end and centrin/CP110 signals at the distal end of centriolar protein complexes was a bit shorter than that of the endogenous procentrioles (n = 7, respectively; Fig 6D). Together, these findings suggest that centriolar protein complexes in RBM14-depleted cells could become the structures more related to procentrioles by incorporating HsSAS-6 and other centriolar proteins although they are still abnormal in length.

To further address this possibility, we ectopically expressed HsSAS-6-GFP in RBM14-depleted cells to see whether there is an increase in the number of centriolar protein complexes recruiting HsSAS-6. Notably, we found that simultaneous HsSAS-6-GFP overexpression and RBM14 depletion synergistically enhanced the frequency of formation of the centriolar protein complexes containing HsSAS-6 foci compared with HsSAS-6-GFP overexpression or RBM14 depletion alone (Supplementary Fig S7A). To strengthen this notion, using long-term fluorescence time-lapse recording, we provided direct evidence that ectopic HsSAS-6-GFP foci assembled in the cytoplasm in ~25% of RBM14-depleted cells, whereas that was rarely the case in control cells (Supplementary Fig S7B and C, and Supplementary Movie S5). Furthermore, we also set up the experimental system in which we could observe the dynamics of both ectopic DsRed-centrin-2 and HsSAS-6-GFP foci in RBM14-depleted cells, and established that incorporation of HsSAS-6-GFP into ectopic DsRed-centrin-2 foci indeed occurred (~16% of ectopic DsRed-centrin-2 foci in RBM14-depleted cells compared with ~3% of those in control cells; Fig 6E and F, and Supplementary Movie S6). Overall, these results suggest that the centriolar protein complexes could serve as a platform to incorporate HsSAS-6 and other centriolar proteins required for the initial stage of procentriole formation. In fact, when the formation of ectopic centriolar protein complexes upon RBM14 depletion was inhibited by concurrent CPAP depletion, the increase of HsSAS-6 foci was significantly suppressed, suggesting that formation of ectopic HsSAS-6 foci is dependent on the existence of ectopic centriolar protein complexes in RBM14-depleted cells (Fig 6G and Supplementary Fig S7D).

Since an extra spindle pole in RBM14-depleted cells likely incorporated ectopic HsSAS-6 and other centriolar proteins aligned in a procentriole-like manner (Fig 6A–G), we hypothesized that the ectopic centriolar protein complexes forming an extra spindle could be structures more akin to procentrioles. To address this possibility, we conducted Live CLEM analysis using HeLa cells expressing GFP-centrin and depleted of RBM14 (Fig 6H, Supplementary Fig S8A–C, and Supplementary Movie S7). In the cells depleted of RBM14, we sometimes observed the pseudo-bipolar spindles in which pre-existing centriole pairs failed to separate each other and organize a single spindle pole while only ectopic GFP-centrin foci assembled the other spindle pole (Fig 6H and Supplementary Figs S6A and S8A–C). Although the reason why pre-existing centriole pairs did not separate in mitosis in such cases remains elusive, we speculate that RBM14 depletion might somewhat disturb the separation of centrosomes. We fixed such cells in which ectopic GFP-centrin foci gathered to assemble a

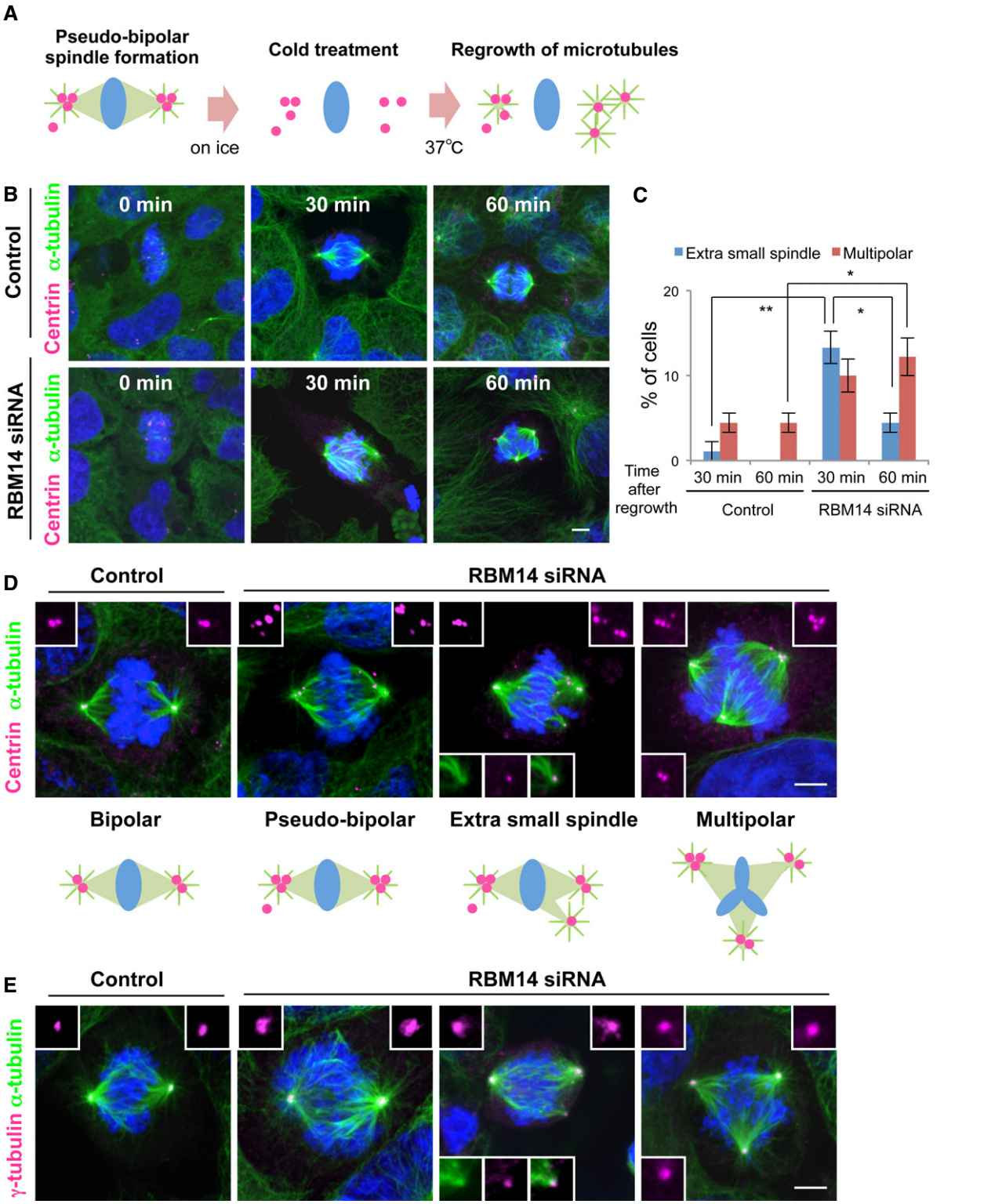

Figure 5. Ectopic centriolar protein complexes can be the sites of microtubule nucleation.

A Schematic of microtubule regrowth assay during mitosis in RBM14-depleted U2OS cells.

B–E Control U2OS cells or U2OS cells treated with siRNA targeting RBM14 were cold-treated for 30 min, followed by 30–60 min incubation at 37°C and stained with antibodies against centrin (magenta in (B) and (D)) or γ-tubulin (magenta in (E)) as well as α-tubulin (green). DNA is shown in blue. Insets show approximately twofold magnified views of fluorescent foci around the centrosome. Scale bar, 5 μm. Histograms represent the percentages of mitotic cells showing the indicated phenotype at each time point. Values are mean percentages ± standard error of mean (SEM) from three independent experiments (n = 30 for each condition). *$P < 0.05$, **$P < 0.01$ (one-tailed t-test).

spindle pole (red arrowheads in Fig 6H, red circle in Supplementary Fig S8C). We then analyzed the structures in those spindle poles by using serial section EM analysis. Although we could not find a cartwheel structure with ninefold symmetrically arranged microtubules, at the spindle pole composed of only ectopic GFP-centrin foci, probably due to technical reasons, we found a single centriole-like structure in a cylindrical arrangement (arrowhead 2 in Fig 6H) as well as other electron-dense structures (arrowheads 1 and 3 in Fig 6H). We also found such centriole-like structures in the daughter cell containing only ectopic GFP-centrin foci (Supplementary Fig S8C). Together, these results support the notion that RBM14 depletion induces ectopic formation of centriolar protein

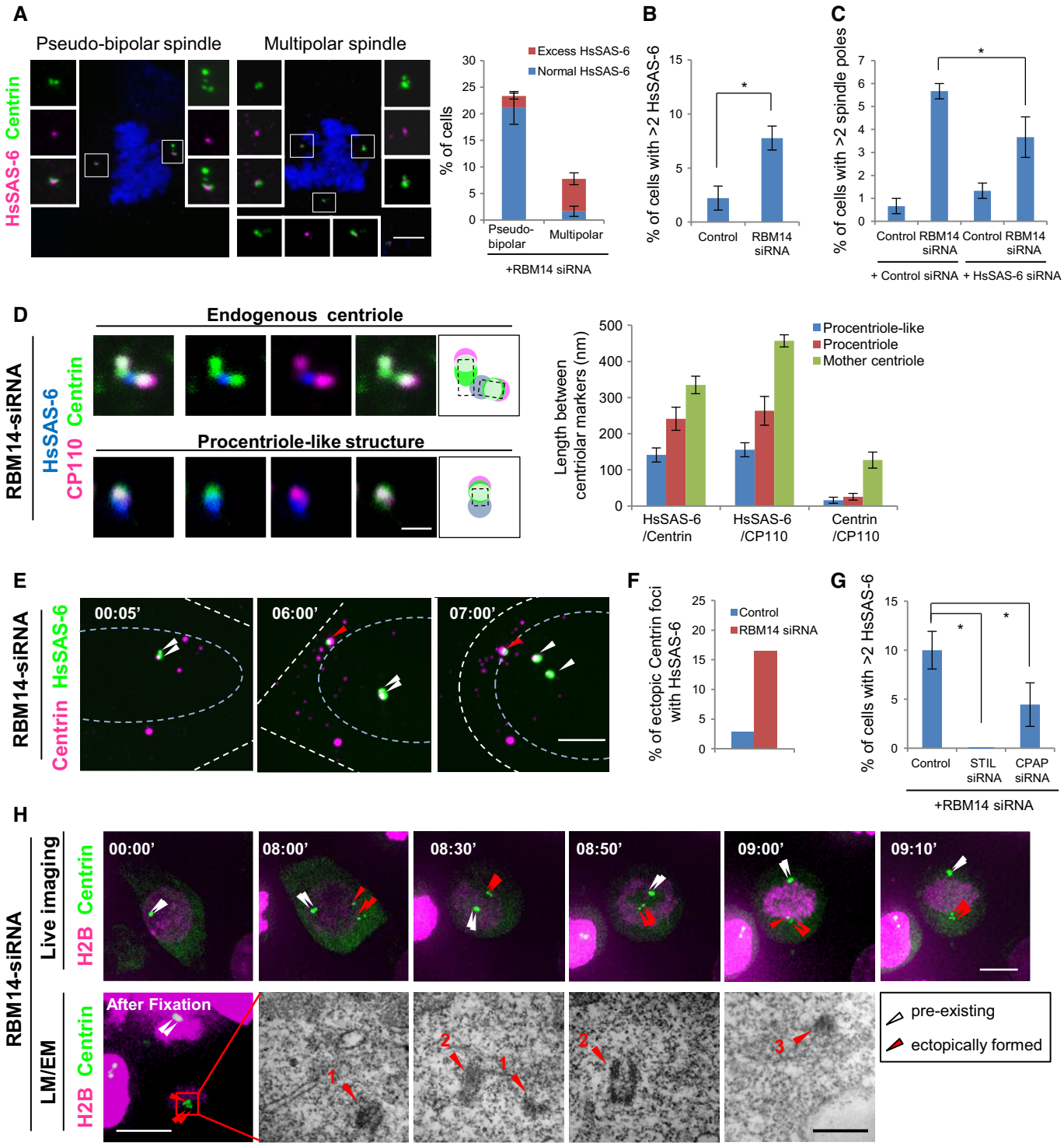

Figure 6.

complexes, a part of which could become a procentriole-like structure even in the presence of pre-existing centrioles.

Discussion

In conclusion, we have, for the first time, identified RBM14 as a suppressor of ectopic assembly of centriolar protein complexes that can function as microtubule organizing centers (MTOCs) (Fig 7). Our work indicates that when RBM14 is depleted, the STIL–CPAP complex can form aberrant centriolar protein complexes in the cytoplasm presumably without assembling a cartwheel structure. Given the heterogeneity of the ectopic structures, there might not be a well-defined order by which centriolar components are incorporated into the structures. As the cell cycle progresses, a part of such centriolar protein complexes seem to assemble into procentriole-like structures that incorporate a set of centriolar proteins required for the initial stage of procentriole formation. We also performed the functional analysis of RBM14 *in vivo* using early mouse embryos and found that RBM14 negatively regulates the assembly of centriolar protein complexes under physiological conditions (Supplementary Fig S9).

How can RBM14 spatiotemporally limit the function of the STIL–CPAP complex? It is possible that RBM14 proteins in the cytoplasm normally suppress STIL function by direct association during interphase. However, in the absence of RBM14, STIL can overly form a complex with CPAP in the cytoplasm, and this complex induces the ectopic formation of centriolar protein complexes during interphase. Considering the observation that overexpression of RBM14-NES which forcibly localized to the cytoplasm, but seemingly not to centrioles, suppressed HU-induced centriole amplification, it is likely that RBM14 acts on cytoplasmic STIL rather than on the STIL implicated in procentriole formation near pre-existing centrioles. Furthermore, given the observation that the STIL/CPAP complex formation was enhanced in the S phase-arrested cells upon treatment with HU (Supplementary Fig S4C), we speculate that RBM14 could inhibit centriole amplification in the S phase-arrested cells by suppressing excess formation of the STIL/CPAP complex in the cytoplasm. By contrast, in the process of canonical centriole formation, formation of the STIL/CPAP complex could be strictly limited in the cytoplasm so as to happen only at the assembly site of procentrioles since RBM14 overexpression had only minor effect on this process in cycling cells (Supplementary Fig S2B). It has been shown that SAS-4/CPAP provides a scaffold for cytoplasmic assembly of PCM components, which implies that PCM assembly could begin in the cytosol before recruitment of this complex to the centrosome (Gopalakrishnan *et al*, 2011). In a similar way, we propose that when RBM14 is depleted, the ectopic STIL/CPAP complex gives a scaffold for assembly of centriolar and PCM components in the cytoplasm and that such complexes including γ-tubulin can be the site to nucleate microtubules during mitosis in RBM14-depleted cells.

Recent studies have shown that depletion of CP110-binding proteins such as Cep76 and Neurl4 induced accumulation of centriolar proteins near pre-existing centrioles and resulted in the formation of the ectopic structures similar to the centriolar protein complexes that we demonstrated in this study (Tsang *et al*, 2009; Li *et al*, 2012). However, the ectopic structures in Cep76-depleted cells contained HsSAS-6 signals, and their formation was HsSAS-6 dependent (Tsang *et al*, 2009). In addition, the ectopic structures disassembled and failed to form a functional microtubule array during mitosis. On the other hand, depletion of Neurl4 led to the formation

Figure 6. Ectopic centriolar protein complexes become the structures more related to procentrioles by incorporating HsSAS-6 and other centriolar proteins.

A U2OS cells treated with RBM14 siRNA and stained with antibodies against centrin-2 (green) as well as HsSAS-6 (magenta). DNA is shown in blue. Insets show approximately twofold magnified views of fluorescent foci around the centrosome. Scale bar, 5 μm. Histograms represent the frequency of mitotic cells with the indicated phenotype. Values are mean percentages ± SEM from three independent experiments (n = 60 for each condition).

B Control U2OS cells or U2OS cells treated with siRNA targeting RBM14 were stained with antibodies against HsSAS-6 as well as centrin-2. Immunofluorescence micrographs are shown in Supplementary Fig S6D. When we counted HsSAS-6 foci in this paper, we only counted cells before metaphase/anaphase transition considering the disappearance of HsSAS-6 from anaphase in mitosis. Histograms represent frequency of mitotic cells with excess foci of the indicated proteins at spindle poles. Values are mean percentages ± SEM from three independent experiments (n = 30 for each condition). *$P < 0.05$ (one-tailed t-test).

C U2OS cells treated with the indicated siRNAs were stained with anti-α-tubulin antibodies and Hoechst 33258. Histograms represent frequency of mitotic cells with the multipolar spindle in the indicated conditions. Values are mean percentages ± SEM from three independent experiments (n = 30 for each condition). *$P < 0.05$ (one-tailed t-test).

D RBM14-depleted HeLa cells expressing GFP-centrin (green) were stained with antibodies against CP110 (magenta) and HsSAS-6 (blue). Scale bar, 1 μm. A representative stained procentriole-like structure as well as endogenous centrioles is shown together with a schematic. Histograms represent length between the centers of the foci of the indicated proteins. Values are mean percentages ± SEM from seven individual cells.

E, F Ectopic DsRed-centrin-2 foci in RBM14-depleted cells recruit HsSAS-6-GFP. (E) Live imaging of RBM14-depleted U2OS cells expressing HsSAS-6-GFP (green) and DsRed-centrin-2 (magenta). Time is denoted in hh:min, and scale bar is 10 μm. Time zero corresponds to the onset of recording. Pre-existing HsSAS-6-GFP foci (white arrowheads) and ectopic HsSAS-6-GFP focus (red arrowhead) were traced throughout the time-lapse recording. White broken lines represent cell shapes, and blue broken lines represent nuclear shapes. (F) Histograms represent the percentages of ectopic DsRed-centrin-2 foci with HsSAS-6-GFP recruitment (n = 69 foci for control, and n = 67 foci for RBM14 siRNA).

G Histograms represent frequency of mitotic cells with excess foci of HsSAS-6 in the indicated conditions. In this experiment, cells were treated with double amount of RBM14 siRNA (20 pmol) compared to that in the other experiments. Values are mean percentages ± SEM from three independent experiments (n = 30 for each condition). *$P < 0.05$ (one-tailed t-test).

H HeLa cells expressing GFP-centrin (green) and RFP-H2B (magenta) and treated with RBM14 siRNA were analyzed using Live CLEM. Pre-existing GFP-centrin foci (white arrowheads) and ectopic GFP-centrin foci (red arrowheads) were traced throughout the time-lapse recording. Z-stacked confocal images spanning the entire height of the cells (< 30 μm) are shown (upper panels). Time is denoted in hh:min. Time zero corresponds to the onset of ectopic formation of GFP-centrin foci. The cells fixed after live imaging were also analyzed for confirming the local correlation between LM and EM images (lower panels). Red square (ectopically formed GFP-centrin foci) represents the region corresponding to that of the EM images acquired from serial sections. Note that ectopic GFP-centrin foci that form a spindle pole include not only electron-dense structures (1, 3) but also a morphologically recognizable centriole-like structure (2). Scale bars, 10 μm (live imaging) and 500 nm (EM).

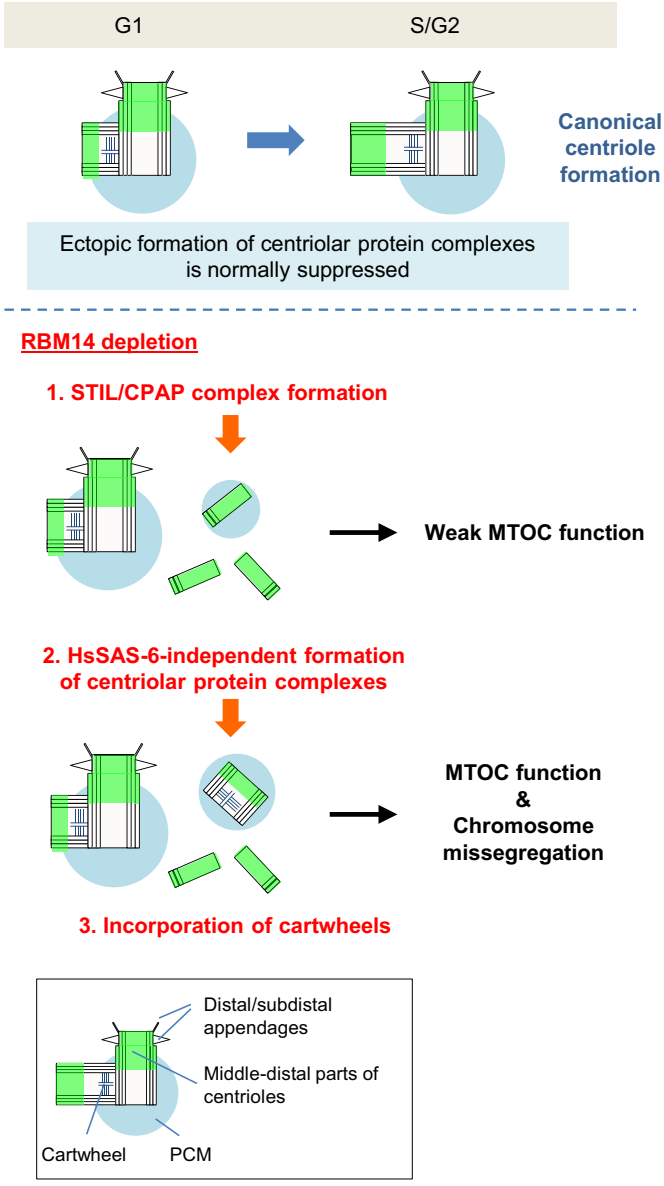

Figure 7. A speculative model for ectopic formation of structures related to centrioles upon RBM14 depletion.
A speculative model suggesting how RBM14 depletion could induce ectopic formation of centriolar protein complexes/procentriole-like structures and affect mitotic spindle integrity. 1. RBM14 depletion leads to the formation of the STIL–CPAP complex in the cytoplasm. 2. Ectopic formation of centriolar protein complexes takes place in the cytoplasm presumably without assembling a cartwheel structure. 3. A part of centriolar protein complexes could assemble into procentriole-like structures that harbor PCM and MTOC function more effectively by incorporating cartwheels.

of centrin-containing ectopic structures without incorporating HsSAS-6 (Li *et al*, 2012), implying that they might be more related to the centriolar protein complexes shown in this study. However, where this assembly takes place in the cells and whether the ectopic structures can finally assemble into the more completed centrioles remains unclear. More recently, it has been reported that depletion of LGALS3BP caused formation of ectopic structures composed of centriolar proteins such as CPAP, acetylated tubulin and centrin (Fogeron *et al*, 2013). However, the formation of those structures was dependent on Plk4, suggesting that the assembly mechanism is different from what is shown in this study.

Further study will be needed to describe the dynamics of the aberrant assembly of centriolar components in more detail and uncover the mechanisms by which they can assemble into substantial and functional structures to efficiently serve as MTOCs. Considering that the ectopic formation of centriolar protein complexes takes place during S phase in RBM14-depleted cells, and also that *de novo* formation of premature centrioles caused by loss of pre-existing centrioles is known to occur during S phase (Khodjakov *et al*, 2002; La Terra *et al*, 2005), there could be a close linkage between the two assembly pathways for centriolar proteins.

Given that RBM14 has been reported as a potential tumor suppressor in human cancer cells (Kang *et al*, 2008), the formation of these structures could contribute to genome instability by inducing chromosome mis-segregation. We speculate that the accumulation of that kind of minor errors could be influential for tumor formation in the long term. Therefore, it will be important to investigate whether such aberrant assembly of centriolar proteins can be a cause of some types of cancer.

Materials and Methods

Cell culture and cell lines

Human U2OS, HEK293T, RPE1, HeLa and HeLa cells stably expressing GFP-centrin 1 (Piel *et al*, 2000), and mouse NIH3T3 cells were cultured in Dulbecco's modified Eagle's medium (DMEM) supplemented with 10% fetal bovine serum (FBS) at 37°C in 5% CO_2 incubator. To generate inducible cell lines, cells were transiently transfected with pEBTet-EGFP-CPAP (Kitagawa *et al*, 2011a) and pEBTet-HsSAS-6-EGFP at 80–90% confluency. 24 h later, cells were exposed to selective medium containing 1 μg/ml puromycin, which led to substantial death of non-transfected cells over 4–5 days. After amplification under selective conditions for 1–2 weeks, cells were frozen in 10% DMSO and stored at −80°C. Expression was induced using 1 μg/ml doxycycline for 24–48 h.

Cell cycle synchronization, cell cycle arrest and FACS analysis

For cell synchronization at G1/S transition, cells were treated with 2 mM thymidine for 16 h, washed twice with phosphate-buffered saline (PBS), released for 8 h in fresh medium without thymidine and treated again with 2 mM thymidine for 16 h. For cell synchronization at G2/M transition, cells were treated with 200 ng/ml nocodazole for 16 h. For cell cycle arrest, cells were treated with 2 mM hydroxyurea (HU) for 16 h for S phase arrest or 25 μM lovastatin for 16 h for G1 phase arrest.

For FACS analysis, cells cultured on dishes were trypsinized, washed twice with PBS and fixed in 70% cold ethanol at −20°C at each time point. The fixed cells were incubated with 0.4 μg/ml RNase for 10 min at 37°C and stained with 100 μg/ml propidium iodide (PI). The DNA contents of the cells were then measured using JSAN desktop cell sorter (Bay Bioscience).

Molecular biology, RNA interference and transfection

The following siRNAs were used: Silencer Select siRNA (Life Technologies) against RBM14 (s20406), mRBM14 (s80246), STIL (s12863), SAS-6 (s46487), CPAP (s31623), NONO (s9614), Cep192 (s30227) and Negative control #1 (4390843); Stealth siRNA (Life Technologies) against 3′ UTR of RBM14 (5′-GCATTCTGGCCAT AGAGCTCGTATT-3′) used in Fig 2A and Negative control Low GC Duplex #2 (12935110); custom siRNA (Sigma Genosys) against 3′ UTR of Plk4 (5′-CTCCTTTCAGACATATAAG-3′).

pcDNA3-FLAG-RBM14 FL and pcDNA3-FLAG-RBM14[N] expression constructs were gifts from Dr. Toshiharu Iwasaki. The expression construct for FLAG-RBM14[C] was created by insertion of the subcloned fragment into HindIII-XhoI site-digested pcDNA3 vector (Invitrogen). The pcDNA3-FLAG-RBM14-NES construct was created by insertion of HIV-Rev NES sequence (LQLPPLERLTLD) onto C-terminus of RBM14. pEGFP-RBM14-PACT was created by insertion of the full-length sequence of RBM14 into the pEGFP-PACT expression vector (gift from Dr. Mikiko Takahashi). pcDNA3-FLAG-RBM14 T1, T2, T3, T4 and ΔTRBP-ID were made from pcDNA3-FLAG-RBM14[C] using Prime STAR MAX mutagenesis Basal kit (TaKaRa). pHA-STIL FL/[N]/[CBD]/[C] expression constructs were created by insertion of subcloned fragments into SpeI-digested pHA vector. The expression construct for RFP-histone H2B was a gift from Dr. Tetsuya Hori. pEBTet-EGFP-CPAP and pEBTet-HsSAS-6-EGFP were created using Gateway System (Invitrogen). pcDNA3-FLAG-Plk4-ΔPEST (Yamashita *et al*, 2001) was a gift from Dr. Hiroyuki Mano. pCMV5-Myc-HsSAS-6 was created by insertion of the subcloned fragment into SalI site-digested pCMV5 vector. The expression construct for DsRed-centrin2 was purchased from Addgene (Plasmid # 29523).

Transfection of siRNA or DNA constructs into U2OS, HeLa, RPE1, HEK293T, and NIH3T3 cells was performed using Lipofectamine RNAiMAX (Life Technologies) or Lipofectamine 2000 (Life Technologies) according to the manufacturer's instruction. Unless otherwise noted, transfected cells were analyzed 72 h after transfection.

Antibodies

The following primary antibodies were used in this study: rabbit polyclonal antibodies against STIL (Abcam, ab89314, IF 1:1,000, WB 1:1,000), RBM14 (Abcam, ab12325, IF 1:300, WB 1:1,000), SAS-6 (Santa Cruz Biotechnology, Inc., sc-98506, IF 1:300, WB 1:1,000), Cep135 (Abcam, ab75005, IF 1:300), Cep192 (a gift from Laurence Pelletier, IF 1:1,000), Cep152 (Bethyl laboratories, A302-480A, IF 1:1,000), CP110 (a gift from Brian David Dynlacht, IF 1:500), CPAP (a gift from Pierre Gönczy, IF 1:500, WB 1:1,000), CPAP/CENP-J (Proteintech, 11517-1-AP, IF 1:500, WB 1:1,000), C-Nap1 (a gift from Erich Nigg, IF 1:1,000), Cep164 (Novus, 45330002, IF 1:500), γ-tubulin (Sigma-Aldrich, T5192, IF 1:1,000), α-tubulin (Abcam, ab18251, IF 1:1,000), centrin-1 (Abcam, ab11257, IF 1:1,000), PCM-1 (Sigma-Aldrich, HPA023370, IF 1:300), GFP (MBL, IF 1:300), FLAG-tag (Sigma-Aldrich, F7425, IF 1:200) and HA-tag (Abcam, ab9110, WB 1:1,000); mouse monoclonal antibodies against centrin-2 (Millipore, 20H5, IF 1:1,000, WB 1:1,000), Centrobin/NIP2 (Abcam, ab70448, IF 1:500), α-tubulin (Sigma-Aldrich, T5168, IF 1:1,000), HsSAS-6 (sc-81431, Santa Cruz Biotechnology, Inc., WB 1:1,000), acetylated tubulin (Sigma-Aldrich, T6793, 6-11B-1, IF 1:1,000), histone H4 (MBL, D214-3, WB 1:1,000) and PCNA (Santa Cruz, sc-56, IF 1:1,000); goat polyclonal antibodies against actin (Santa Cruz Biotechnology, Inc., ac-1616, WB 1:1,000); and goat polyclonal antibody against GFP, FITC-conjugated (Abcam, ab6662, IF 1:300).

The following secondary antibodies were used: Alexa Fluor 488 goat anti-mouse IgG (H+L) (Molecular Probes, 1:500), Alexa Fluor 568 goat anti-rabbit IgG (H+L) (Molecular Probes, 1:500) and goat polyclonal antibody against mouse IgG (H+L)-CY5 (Abcam, ab6563, 1:500) for IF and goat polyclonal antibodies HRP against mouse IgG (Promega, W402B, 1:5,000), rabbit IgG (Promega, W401B, 1:5,000) and HRP-labeled protein A (KPL, 14-50-00, WB: 1:2,500) for WB.

Indirect immunofluorescence and immunoblotting

For indirect immunofluorescence microscopy, the cells cultured on coverslips were fixed using −20°C methanol for 10 min. The cells were then permeabilized with PBS/0.05% Triton X-100 (PBSX) for 5 min, washed with PBS three times and incubated for blocking in 1% BSA in PBSX for 30 min at 37°C. The cells were then incubated with primary antibodies for 1 h at 37°C, washed with PBSX three times and incubated with secondary antibodies for 1 h at 37°C. The cells were thereafter washed with PBSX twice, stained with 1 μg/ml Hoechst 33258 in PBS for 5 min at RT, washed again with PBSX and mounted onto glass slide. Counting the number of immunofluorescence signals was performed using an Axioplan2 fluorescence microscope (Carl Zeiss) with a 100×/1.4 NA plan-APOCHROMAT objective. Confocal images were recorded using a Fluoview FV-1000D confocal laser scanning microscope system (Olympus) with a 100×/1.4 NA UPlanSApo objective and analyzed using FV10-ASM software (Olympus) and Adobe Photoshop.

For the preparation of human soluble cytosolic fractions for immunoblotting, cells were collected, washed in PBS and lysed on ice for 30 min in lysis buffer [20 mM Tris–HCl pH 7.5, 100 mM NaCl, 1 mM EDTA, 1 mM DTT, 0.5% NP-40 and 1/1,000 protease inhibitor cocktail (nacalai tesque)]. Lysates were cleared by centrifugation for 15 min at 16,000 *g* at 4°C and the supernatant collected. SDS–PAGE was performed using 8–12% polyacrylamide gels, followed by transfer on Immobilon-P membrane (Millipore corporation). The membrane was probed with the primary antibodies, followed by incubation with their respective HRP-conjugated secondary antibodies (Promega). Washes were performed in PBS containing 0.02% Tween (PBST). The signal was detected as chemiluminescence (GE healthcare, ECL Prime). Signal intensity of immuno-reactive bands was measured using ImageJ software (http://rsb.info.nih.gov/ij/).

Electron microscopy/Correlative light and electron microscopy (CLEM)

For electron microscopy, the cells cultured on 6-well dishes were washed with PBS and fixed with 2% glutaraldehyde and 1.5% Tannic Acid in PBS for 1 h. The cells were postfixed with 1% OsO_4 for 1 h on ice and stained with 1% uranyl acetate for 30 min on ice. The samples were then dehydrated and embedded in Quetol 812 (Nisshin EM). Ultrathin sections were post-stained with 7% aqueous uranyl acetate for 20 min and 0.8% lead citrate for 2 min and then observed by a transmission electron microscope JEM-1010 (JEOL). Images were acquired with a VELETA CCD camera (SEIKA Corporation)

and analyzed with iTEM software (SEIKA Corporation) and Adobe Photoshop.

For CLEM, U2OS cells expressing GFP-CPAP were cultured on 35-mm glass-bottom dishes with grid (MatTek Co., P35G-2-14-C-GRID). The cells were fixed with 4% paraformaldehyde 24 h after transfection with RBM14 siRNA and induction of GFP-CPAP. Fluorescence microscopy was performed on a Cell Voyager CV1000 Confocal Scanner Box (Yokogawa Electric Co.) with a 63× oil immersion objective. After fixation and dehydration as described above, the cells were embedded in Quetol 812 by inverting the Quetol 812-filled beam capsules onto the glass-bottom dishes. The regions including the cells of interest were found by a grid reference using stereoscopic microscope. Ultra-thin sectioning and following staining were performed as described above.

Immunoprecipitation and mass spectrometry

For preparing soluble cytosolic fractions of HeLa, U2OS or HEK293T cells, cells were washed by PBS and lysed in ice-cold lysis buffer. The lysates were vortexed for 15 min at 4°C, and insoluble material was removed after centrifugation for 15 min. For STIL immunoprecipitation, soluble cytosolic fractions of HeLa, HEK293T or U2OS cells were incubated with protein A agarose for 1 h at 4°C for preclear and then incubated for 2 h at 4°C with protein A agarose that had been incubated with anti-STIL antibodies or normal rabbit IgG for mock immunoprecipitation. The beads were washed at least three times with lysis buffer and resuspended in SDS-sample buffer before loading onto a SDS–PAGE gel. To identify STIL-interacting proteins, the gel stained with SimplyBlue™ Safe (Invitrogen) was cut into five pieces. The peptides were digested in gel by trypsin and extracted from the gel. The peptides were subsequently desalted and analyzed by a HCT-Ion trap mass spectrometer (Bruker Daltonik GmbH).

For co-immunoprecipitation assays, the lysates of HEK293T cells transfected with the indicated plasmids (pcDNA3-FLAG-RBM14 FL/[N]/[C], pHA-STIL FL/[N]/[C]) for 24 h were lysed in ice-cold lysis buffer and incubated with anti-FLAG M2 agarose beads (Sigma-Aldrich, A2220) for 2 h at 4°C. The beads were then washed three times with ice-cold lysis buffer and resuspended in SDS-sample buffer.

GST pull-down assay and *in vitro* competitive binding assay

DNA encoding fragments of human STIL or RBM14 were cloned in pGEX system vectors (GE healthcare) encoding for GST-tags. DNA encoding fragments of CPAP[SBD] were cloned into pET30a vector encoding for His-tags. The recombinant protein expression of the fragments was performed in *E. coli* strain BL21-Gold (DE3) in LB medium. Protein expression was induced at 22°C by addition of 0.3 mM IPTG and allowed to proceed for 18 h. Cell pellets expressing GST-STIL and RBM14 were lysed by lysozyme treatment and sonication and resuspended in lysis buffer containing 50 mM Tris–HCl (pH 7.5), 500 mM NaCl, 5 mM EDTA, 1 mM DTT, 1:1,000 protease inhibitor cocktail (Sigma) and 0.5% Triton X-100. The lysates were incubated with Glutathione sepharose beads (GE healthcare). The beads were then washed ten times with lysis buffer supplemented with additional 500 mM NaCl. For preparing N-terminal fragment of STIL, proteins were eluted from the beads by removal of the GST-tags by prescission protease (GE healthcare) in a buffer containing 20 mM Tris–HCl (pH 7.5), 150 mM NaCl, 0.5 mM EDTA and 1 mM DTT. Cell pellets expressing His-CPAP[SBD] were lysed by lysozyme treatment and sonication and resuspended in lysis buffer containing 50 mM Tris–HCl (pH 7.5), 500 mM NaCl, 20 mM imidazole and 0.5% Triton X-100. The lysates were incubated with Ni-NTA agarose beads (QIAGEN). The beads were then washed ten times with lysis buffer. Proteins were eluted from the beads with a buffer containing 80 mM PIPES-KOH (pH 6.8), 80 mM KCl, 2 mM $MgCl_2$ and 400 mM imidazole.

For GST pull-down assays, the Glutathione sepharose beads which retain bacterially purified GST-RBM14 fragments were resuspended in ice-cold lysis buffer and incubated with ~5 μg bacterially purified N-terminal fragment of STIL for 2 h at 4°C. The resin was washed five times with ice-cold lysis buffer and resuspended in SDS-sample buffer. Proteins were separated by SDS–PAGE and stained with SimplyBlue™ Safe (Invitrogen). For *in vitro* competitive binding assays, the GST pull-down experiment was performed in the same way with purified STIL[N] and GST-RBM14[C] in the presence of the indicated amount of purified His-CPAP[SBD] in Fig 3E.

Yeast two-hybrid analysis

Yeast strain MAV103 was grown in YPD medium and transformed with a modified version of the vectors pPC86 and pPC97 (Clontech) that contained full-length or fragments of RBM14 or STIL. Positive colonies were cultured in yeast dropout medium without leucine (L) and tryptophan (W) overnight. On the next day, cells were diluted to an $OD_{600} = 1$. 10 μl of this solution was spotted on yeast (−L/−W) plates supplemented with 50 mM 3-amino-triazol. Two serial dilutions to an OD of 0.1 and 0.01 were prepared, and 10 μl of these dilutions was spotted as well. Plates were placed at 30°C until clear colonies had formed on a positive control, which was SAS-6 coiled-coil self-interaction in the initial experiments.

Time-lapse fluorescence microscopy and image analysis

Time-lapse fluorescence microscopy was performed on a Cell Voyager CV1000 Confocal Scanner Box with a 63× oil immersion objective in an equilibrated chamber in 5% CO_2 at 37°C. HeLa cells stably expressing GFP-centrin1 were cultured on 35-mm glass-bottom dishes (MatTek Co.), and they were transfected with RBM14 siRNA or control siRNA together with a plasmid DNA coding RFP-histone H2B. U2OS cells expressing HsSAS-6-GFP were cultured in the same way and transfected with RBM14 siRNA or control siRNA together with or without a pDsRed-N1-Centrin2 vector. After 1 day, the U2OS cells were then treated with 1 μg/ml doxycycline and/or 6 μM aphidicolin. After 2 days from transfection, the cells were analyzed by fluorescence and bright field microscopy every 5 or 10 min over 24–48 h. After time-lapse recording, we generated the movies and figure panels by using Z-stack images from 25 to 30 Z-planes covering approximately the whole height of the cells along the *z*-axis to capture fluorescent foci that move extensively in all three dimensions. For quantification of the number of fluorescent foci and their intensity, the acquired sequential TIFF files were analyzed using ImageJ software (http://rsb.info.nih.gov/ij/).

Live correlative light and electron microscopy (Live CLEM)

For Live CLEM, the cells were cultured on 35-mm glass-bottom dishes with grid. We treated RBM14-depleted cells with a moderate concentration of monastrol (50 μM) for 12 h to arrest the cells in mitosis and select the cells which harbor extra mitotic spindle poles containing only ectopic centrin foci although not all cells responded to that concentration of the drug in our experimental condition (Fig 6H, Supplementary Fig S8A and B, and Supplementary Movie S7, but no monastrol treatment for the experiment in Supplementary Fig S8C). The cells were thereafter observed by time-lapse fluorescence microscopy as described above. We also acquired immunofluorescence images of paraformaldehyde-fixed cells after the time-lapse recording as individual GFP-centrin foci correspond to the structures on EM images precisely in the same location. Then, we performed CLEM analysis as described in the method of CLEM.

RNAi experiments in mouse early embryos

Capped synthetic mRNAs were transcribed with the use of a mMessage mMachine kit (Ambion) using pCS2 tdTomato and pCS2 memTomato which consisted of tdTomato and the NH_2-terminal sequence of neuromodulin (nucleotides 679–738) from pECFP-mem (BD Biosciences). For single-cell injection, we used a Leica DMIRB microscope (Leica Microsystems), manipulators with Femto jet (Eppendorf) and piezo-xpert (Eppendorf). The injection was performed in modified Whitten's medium (mWM). Fertilized eggs were obtained by mating CMV-EGFP::centrin2 transgenic male (Higginbotham *et al*, 2004) with superovulated female mice. Single blastomeres of 8–16 cell embryos were injected with 16 μM Silencer Select siRNA (Life Technologies) against mRBM14 (s80246) or negative control #1 (4390843), and fluorescence mRNA. Injected embryos were cultured for 40 h in mWM solution in a 5% CO_2 incubator and checked under M205FA fluorescence stereo microscope (Leica Microsystems). Only embryos that had Tomato and GFP expression were observed with FV1000 confocal microscope (Olympus).

For immunofluorescence analysis, embryos were recovered in PBS. They were carefully staged on the basis of their morphology. They were dehydrated with methanol series and were fixed overnight at 4°C in 100% methanol, washed twice with PBS and incubated for 1 h at 4°C with TSA blocking reagent (Perkin-Elmer). Immunostaining was performed with rabbit antibodies against RBM14 (Abcam, ab12325, 1:50) and Alexa Fluor 647-conjugated chick antibodies to rabbit immunoglobulin G (Invitrogen). Samples were washed with PBS between staining steps. Nuclei were stained by incubation for 30 min with 4′,6-diamidino-2-phenylindole dihydrochloride (1/2,000 dilution in PBS, Wako). Images were obtained using FV1000 confocal microscope (Olympus).

Supplementary information for this article is available online: http://emboj.embopress.org

Acknowledgements

We are grateful to Diego Chiappe and Marc Moniatte (Proteomic core facility, School of Life Sciences, EPFL) for mass spectrometry, to Michel Bornens for HeLa cells stably expressing GFP-centrin1, to Erich Nigg for C-Nap1 antibodies, to Laurence Pelletier for Cep192 antibodies, to Brian David Dynlacht for CP110 antibodies, to Emiko Suzuki for supporting EM analysis, to Tetsuya Hori and Tatsuo Fukagawa for supporting live cell imaging and a construct coding RFP-H2B, to Toshiharu Iwasaki and Eli Lilly and company for a construct coding RBM14, to Hiroyuki Mano for a construct coding Plk4, to Mikiko Takahashi for a construct coding PACT as well as to Midori Ota and Rieko Matsuura for critical reading of the manuscript. We thank Pierre Gönczy for CPAP antibodies, constructs and fruitful discussions. This work was supported by Grant-in-Aid for JSPS Fellows, Grant-in-Aid for Young Scientists (A) and for Scientific Research on Innovative Areas from the Ministry of Education, Science, Sports and Culture of Japan, by Improvement of Research environment for young researchers Grant from JST, by the Uehara Memorial Foundation, by Takeda Science Foundation, by the Mitsubishi foundation, by Mochida Memorial Foundation for Medical and Pharmaceutical Research, by Astellas Foundation for Research on Metabolic Disorders, by The Sagawa Foundation for Promoting Cancer Research, by Novartis Foundation for the Promotion of Science, by the Center for the Promotion of Integrated Sciences of Sokendai and by the Trans-disciplinary Research Integration center.

Author contributions

GS and DK designed the study; GS, TA and DK performed experiments; KT and HH performed *in vivo* mouse experiments; GS and DK designed experiments and analyzed data; GS, KT and DK wrote the manuscript, which was commented on by all authors.

Conflict of interest

The authors declare that they have no conflict of interest.

References

Arquint C, Sonnen KF, Stierhof YD, Nigg EA (2012) Cell-cycle-regulated expression of STIL controls centriole number in human cells. *J Cell Sci* 125: 1342 – 1352

Auboeuf D, Dowhan DH, Li X, Larkin K, Ko L, Berget SM, O'Malley BW (2004) CoAA, a nuclear receptor coactivator protein at the interface of transcriptional coactivation and RNA splicing. *Mol Cell Biol* 24: 442 – 453

Balczon R, Bao L, Zimmer WE (1994) PCM-1, A 228-kD centrosome autoantigen with a distinct cell cycle distribution. *J Cell Biol* 124: 783 – 793

Blachon S, Gopalakrishnan J, Omori Y, Polyanovsky A, Church A, Nicastro D, Malicki J, Avidor-Reiss T (2008) *Drosophila* asterless and vertebrate Cep152 Are orthologs essential for centriole duplication. *Genetics* 180: 2081 – 2094

van Breugel M, Hirono M, Andreeva A, Yanagisawa HA, Yamaguchi S, Nakazawa Y, Morgner N, Petrovich M, Ebong IO, Robinson CV, Johnson CM, Veprintsev D, Zuber B (2011) Structures of SAS-6 suggest its organization in centrioles. *Science* 331: 1196 – 1199

Brito DA, Gouveia SM, Bettencourt-Dias M (2012) Deconstructing the centriole: structure and number control. *Curr Opin Cell Biol* 24: 4 – 13

Chen Z, Indjeian VB, McManus M, Wang L, Dynlacht BD (2002) CP110, a cell cycle-dependent CDK substrate, regulates centrosome duplication in human cells. *Dev Cell* 3: 339 – 350

Courtois A, Hiiragi T (2012) Gradual meiosis-to-mitosis transition in the early mouse embryo. *Results Probl Cell Differ* 55: 107 – 114

Culver BP, Meehl JB, Giddings TH Jr, Winey M (2009) The two SAS-6 homologs in Tetrahymena thermophila have distinct functions in basal body assembly. *Mol Biol Cell* 20: 1865 – 1877

Dammermann A, Muller-Reichert T, Pelletier L, Habermann B, Desai A, Oegema K (2004) Centriole assembly requires both centriolar and pericentriolar material proteins. *Dev Cell* 7: 815 – 829

Delattre M, Leidel S, Wani K, Baumer K, Bamat J, Schnabel H, Feichtinger R, Schnabel R, Gönczy P (2004) Centriolar SAS-5 is required for centrosome duplication in *C. elegans*. *Nat Cell Biol* 6: 656 – 664

Delattre M, Canard C, Gönczy P (2006) Sequential protein recruitment in C. elegans centriole formation. *Curr Biol* 16: 1844 – 1849

Dzhindzhev NS, Yu QD, Weiskopf K, Tzolovsky G, Cunha-Ferreira I, Riparbelli M, Rodrigues-Martins A, Bettencourt-Dias M, Callaini G, Glover DM (2010) Asterless is a scaffold for the onset of centriole assembly. *Nature* 467: 714 – 718

Fogeron ML, Muller H, Schade S, Dreher F, Lehmann V, Kuhnel A, Scholz AK, Kashofer K, Zerck A, Fauler B, Lurz R, Herwig R, Zatloukal K, Lehrach H, Gobom J, Nordhoff E, Lange BM (2013) LGALS3BP regulates centriole biogenesis and centrosome hypertrophy in cancer cells. *Nat Commun* 4: 1531

Fox AH, Lam YW, Leung AK, Lyon CE, Andersen J, Mann M, Lamond AI (2002) Paraspeckles: a novel nuclear domain. *Curr Biol* 12: 13 – 25

Fry AM, Mayor T, Meraldi P, Stierhof YD, Tanaka K, Nigg EA (1998) C-Nap1, a novel centrosomal coiled-coil protein and candidate substrate of the cell cycle-regulated protein kinase Nek2. *J Cell Biol* 141: 1563 – 1574

Gomez-Ferreria MA, Rath U, Buster DW, Chanda SK, Caldwell JS, Rines DR, Sharp DJ (2007) Human Cep192 is required for mitotic centrosome and spindle assembly. *Curr Biol* 17: 1960 – 1966

Gönczy P (2012) Towards a molecular architecture of centriole assembly. *Nat Rev Mol Cell Biol* 13: 425 – 435

Gopalakrishnan J, Mennella V, Blachon S, Zhai B, Smith AH, Megraw TL, Nicastro D, Gygi SP, Agard DA, Avidor-Reiss T (2011) Sas-4 provides a scaffold for cytoplasmic complexes and tethers them in a centrosome. *Nat Commun* 2: 359

Graser S, Stierhof YD, Lavoie SB, Gassner OS, Lamla S, Le Clech M, Nigg EA (2007) Cep164, a novel centriole appendage protein required for primary cilium formation. *J Cell Biol* 179: 321 – 330

Higginbotham H, Bielas S, Tanaka T, Gleeson JG (2004) Transgenic mouse line with green-fluorescent protein-labeled Centrin 2 allows visualization of the centrosome in living cells. *Transgenic Res* 13: 155 – 164

Hung LY, Tang CJ, Tang TK (2000) Protein 4.1 R-135 interacts with a novel centrosomal protein (CPAP) which is associated with the gamma-tubulin complex. *Mol Cell Biol* 20: 7813 – 7825

Iwasaki T, Chin WW, Ko L (2001) Identification and characterization of RRM-containing coactivator activator (CoAA) as TRBP-interacting protein, and its splice variant as a coactivator modulator (CoAM). *J Biol Chem* 276: 33375 – 33383

Kang YK, Schiff R, Ko L, Wang T, Tsai SY, Tsai MJ, O'Malley BW (2008) Dual roles for coactivator activator and its counterbalancing isoform coactivator modulator in human kidney cell tumorigenesis. *Cancer Res* 68: 7887 – 7896

Khodjakov A, Rieder CL, Sluder G, Cassels G, Sibon O, Wang CL (2002) De novo formation of centrosomes in vertebrate cells arrested during S phase. *J Cell Biol* 158: 1171 – 1181

Kilburn CL, Pearson CG, Romijn EP, Meehl JB, Giddings TH Jr, Culver BP, Yates JR 3rd, Winey M (2007) New Tetrahymena basal body protein components identify basal body domain structure. *J Cell Biol* 178: 905 – 912

Kitagawa D, Busso C, Fluckiger I, Gönczy P (2009) Phosphorylation of SAS-6 by ZYG-1 is critical for centriole formation in C. elegans embryos. *Dev Cell* 17: 900 – 907

Kitagawa D, Kohlmaier G, Keller D, Strnad P, Balestra FR, Fluckiger I, Gönczy P (2011a) Spindle positioning in human cells relies on proper centriole formation and on the microcephaly proteins CPAP and STIL. *J Cell Sci* 124: 3884 – 3893

Kitagawa D, Vakonakis I, Olieric N, Hilbert M, Keller D, Olieric V, Bortfeld M, Erat MC, Flückiger I, Gönczy P, Steinmetz MO (2011b) Structural basis of the 9-fold symmetry of centrioles. *Cell* 144: 364 – 375

Kleylein-Sohn J, Westendorf J, Le Clech M, Habedanck R, Stierhof YD, Nigg EA (2007) Plk4-induced centriole biogenesis in human cells. *Dev Cell* 13: 190 – 202

Kohlmaier G, Loncarek J, Meng X, McEwen BF, Mogensen MM, Spektor A, Dynlacht BD, Khodjakov A, Gönczy P (2009) Overly long centrioles and defective cell division upon excess of the SAS-4-related protein CPAP. *Curr Biol* 19: 1012 – 1018

La Terra S, English CN, Hergert P, McEwen BF, Sluder G, Khodjakov A (2005) The de novo centriole assembly pathway in HeLa cells: cell cycle progression and centriole assembly/maturation. *J Cell Biol* 168: 713 – 722

Leidel S, Delattre M, Cerutti L, Baumer K, Gönczy P (2005) SAS-6 defines a protein family required for centrosome duplication in *C. elegans* and in human cells. *Nat Cell Biol* 7: 115 – 125

Li J, Kim S, Kobayashi T, Liang FX, Korzeniewski N, Duensing S, Dynlacht BD (2012) Neurl4, a novel daughter centriole protein, prevents formation of ectopic microtubule organizing centres. *EMBO Rep* 13: 547 – 553

Marshall WF, Vucica Y, Rosenbaum JL (2001) Kinetics and regulation of de novo centriole assembly. Implications for the mechanism of centriole duplication. *Curr Biol* 11: 308 – 317

Nakazawa Y, Hiraki M, Kamiya R, Hirono M (2007) SAS-6 is a cartwheel protein that establishes the 9-fold symmetry of the centriole. *Curr Biol* 17: 2169 – 2174

Nigg EA, Raff JW (2009) Centrioles, centrosomes, and cilia in health and disease. *Cell* 139: 663 – 678

Peel N, Stevens NR, Basto R, Raff JW (2007) Overexpressing centriole-replication proteins in vivo induces centriole overduplication and de novo formation. *Curr Biol* 17: 834 – 843

Pelletier L, O'Toole E, Schwager A, Hyman AA, Muller-Reichert T (2006) Centriole assembly in Caenorhabditis elegans. *Nature* 444: 619 – 623

Piel M, Meyer P, Khodjakov A, Rieder CL, Bornens M (2000) The respective contributions of the mother and daughter centrioles to centrosome activity and behavior in vertebrate cells. *J Cell Biol* 149: 317 – 330

Rodrigues-Martins A, Riparbelli M, Callaini G, Glover DM, Bettencourt-Dias M (2007) Revisiting the role of the mother centriole in centriole biogenesis. *Science* 316: 1046 – 1050

Sasaki YT, Ideue T, Sano M, Mituyama T, Hirose T (2009) MENepsilon/beta noncoding RNAs are essential for structural integrity of nuclear paraspeckles. *Proc Natl Acad Sci USA* 106: 2525 – 2530

Schmidt TI, Kleylein-Sohn J, Westendorf J, Le Clech M, Lavoie SB, Stierhof YD, Nigg EA (2009) Control of centriole length by CPAP and CP110. *Curr Biol* 19: 1005 – 1011

Stearns T, Evans L, Kirschner M (1991) Gamma-tubulin is a highly conserved component of the centrosome. *Cell* 65: 825 – 836

Stevens NR, Dobbelaere J, Brunk K, Franz A, Raff JW (2010a) *Drosophila* Ana2 is a conserved centriole duplication factor. *J Cell Biol* 188: 313 – 323

Stevens NR, Roque H, Raff JW (2010b) DSas-6 and Ana2 coassemble into tubules to promote centriole duplication and engagement. *Dev Cell* 19: 913 – 919

Strnad P, Leidel S, Vinogradova T, Euteneuer U, Khodjakov A, Gönczy P (2007) Regulated HsSAS-6 levels ensure formation of a single procentriole per centriole during the centrosome duplication cycle. *Dev Cell* 13: 203 – 213

Tang CJ, Fu RH, Wu KS, Hsu WB, Tang TK (2009) CPAP is a cell-cycle regulated protein that controls centriole length. *Nat Cell Biol* 11: 825 – 831

Tang CJ, Lin SY, Hsu WB, Lin YN, Wu CT, Lin YC, Chang CW, Wu KS, Tang TK (2011) The human microcephaly protein STIL interacts with CPAP and is required for procentriole formation. *EMBO J* 30: 4790 – 4804

Tsang WY, Spektor A, Vijayakumar S, Bista BR, Li J, Sanchez I, Duensing S, Dynlacht BD (2009) Cep76, a centrosomal protein that specifically restrains centriole reduplication. *Dev Cell* 16: 649 – 660

Vulprecht J, David A, Tibelius A, Castiel A, Konotop G, Liu F, Bestvater F, Raab MS, Zentgraf H, Izraeli S, Kramer A (2012) STIL is required for centriole duplication in human cells. *J Cell Sci* 125: 1353 – 1362

Yabe T, Ge X, Pelegri F (2007) The zebrafish maternal-effect gene cellular atoll encodes the centriolar component sas-6 and defects in its paternal function promote whole genome duplication. *Dev Biol* 312: 44 – 60

Yamashita Y, Kajigaya S, Yoshida K, Ueno S, Ota J, Ohmine K, Ueda M, Miyazato A, Ohya K, Kitamura T, Ozawa K, Mano H (2001) Sak serine-threonine kinase acts as an effector of Tec tyrosine kinase. *J Biol Chem* 276: 39012 – 39020

Zheng Y, Jung MK, Oakley BR (1991) Gamma-tubulin is present in Drosophila melanogaster and Homo sapiens and is associated with the centrosome. *Cell* 65: 817 – 823

Zhu F, Lawo S, Bird A, Pinchev D, Ralph A, Richter C, Müller-Reichert T, Kittler R, Hyman AA, Pelletier L (2008) The mammalian SPD-2 ortholog Cep192 regulates centrosome biogenesis. *Curr Biol* 22: 136 – 141

Zou C, Li J, Bai Y, Gunning WT, Wazer DE, Band V, Gao Q (2005) Centrobin: a novel daughter centriole-associated protein that is required for centriole duplication. *J Cell Biol* 171: 437 – 445